

Modeling Epidermis Homeostasis and Psoriasis Pathogenesis

Hong Zhang (张红)^{1,2,*} Wenhong Hou (侯文洪)^{1,*} Laurence Henrot,³ Marc Dumas,⁴ Sylvianne Schnebert,⁴ Catherine Heus,⁴ and Jin Yang (杨劲)^{1,†}

¹*CAS-MPG Partner Institute and Key Laboratory for Computational Biology, Shanghai Institutes for Biological Sciences, Shanghai 200031, China*

²*Naval Submarine Academy, Qingdao, Shandong 266000, China*

³*Sprim Advanced Life Sciences, 1 Daniel Burnham Court, San Francisco, CA 94109, USA*

⁴*LVMH Research, 185 Avenue de Verdun, 45804, Saint-Jean-de-Braye, France*

(Dated: February 27, 2022)

We present a computational model to study the spatiotemporal dynamics of the epidermis homeostasis under normal and pathological conditions. The model consists of a population kinetics model of the central transition pathway of keratinocyte proliferation, differentiation and loss and an agent-based model that propagates cell movements and generates the stratified epidermis. The model recapitulates observed homeostatic cell density distribution, the epidermal turnover time and the multilayered tissue structure. We extend the model to study the onset, recurrence and phototherapy-induced remission of psoriasis. The model considers the psoriasis as a parallel homeostasis of normal and psoriatic keratinocytes originated from a shared stem-cell niche environment and predicts two homeostatic modes of the psoriasis: a disease mode and a quiescent mode. Interconversion between the two modes can be controlled by interactions between psoriatic stem cells and the immune system and by the normal and psoriatic stem cells competing for growth niches. The prediction of a quiescent state potentially explains the efficacy of the multi-episode UVB irradiation therapy and recurrence of psoriasis plaques, which can further guide designs of therapeutics that specifically target the immune system and/or the keratinocytes.

Keywords: Mathematical model, Epidermal homeostasis, Psoriasis, Bimodal switch, Immune system

I. INTRODUCTION

The epidermis, the outermost layer of skin, provides the human body a physiological barrier to the environment and protects the body from water loss, pathogenic infection and physical injury. The epidermis organizes into a stratified structure of keratinocytes at several differentiated stages [1], which constitute 95% cell population in the epidermis [2]. Like other regenerative tissues, the epidermis constantly renews itself to replace desquamated and apoptotic keratinocytes, repair tissue damage and establish the homeostasis. The renewal is orchestrated by a cascade of cellular processes including proliferation, differentiation, migration, apoptosis and desquamation [3–5]. A keratinocyte transits spatially from the stratum basale to the stratum corneum during its lifespan and meanwhile experiences multi-stage biochemical and morphological changes. Many endogenous and exogenous factors (e.g., Ca^{2+} concentration, cytokines, UV irradiation, etc.) affect the epidermal dynamics and the homeostasis of the epidermis by regulating one or more cellular processes.

Mathematical and computational models have long been useful tools to predict cellular behaviors of the epidermis renewal under normal or pathological conditions. Previous models for the epidermal dynamics usually adopted two approaches. One approach includes deterministic models that derived analytical solutions to stationary cell populations. For example, the model by Savill [6] described proliferation

of stem cells and transit-amplifying cells and differentiation to post-mitotic cells, which predicted the influences of apoptosis, cell-cycle time and transit time on cell populations. Gandolfi et al. [7] proposed a spatiotemporal model to investigate the evolution of epidermis, which described cell motion by a constitutive equation. The other approach includes agent-based models that treat individual keratinocytes as computing entities operating under specific physical and biological rules. Such models can simulate the multi-layer epidermal structure organized by cell proliferation, differentiation, death and migration, in which nonspecific intracellular and extracellular biochemical factors affected cell proliferation and differentiation while physical adhesive and repulsive forces governed cell motion [8–12].

In this paper, we present a hybrid model to combine advantages of the above two approaches. The model uses a mean-field cell population kinetics together with an agent-based model for cell migration. The model computes population dynamics of the epidermal renewal without having to compute the cell movements simultaneously, allowing fast and analytical evaluations of modeling hypotheses and results. The population kinetics model describes cellular processes including cell division, differentiation, apoptosis and desquamation. Either deterministic or stochastic simulation can be used to generate the population dynamics of keratinocytes. The cell migration is described by a two-dimensional agent-based model that tracks the cell movement driven by cell-cell interactions. Simulation of the cell migration can be integrated with the stochastic population dynamics to visualize the tissue stratification and establishment of homeostasis. A properly parameterized model reproduces experimentally-observed epidermis growth, differentiation and desquamation dynamics, homeostatic density distribution over different types of keratinocytes and the epidermis turnover times of different cell compartments.

* These authors contributed equally

† Correspondence. 320 Yue Yang Road, Shanghai 200031, China. Tel: +86-21-54920476; Fax: +86-21-54920451; E-Mail: jinyang2004@gmail.com

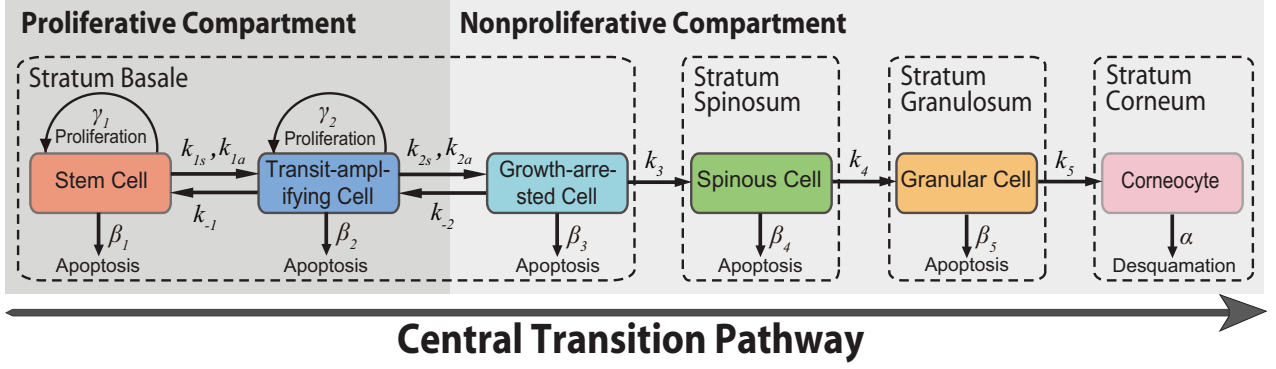


FIG. 1. **The central transition pathway of the epidermis renewal.** The model describes proliferating and nonproliferating keratinocytes. Stem cells and transit amplifying cells proliferate by self-renewal and by symmetric division and asymmetric division. The transit-amplifying cells differentiate into the growth-arrested cells in the nonproliferative compartment, which in turn differentiate into keratinocytes of later stages, including spinous cells, granular cells and corneocytes. Nucleated cells undergo apoptosis and corneocytes desquamate from the stratum corneum. All cellular processes are parameterized by rate constants labeled on transitions.

To investigate an important pathological condition of the skin, we study the onset and recurrence of psoriasis plaques and their recovery under the phototherapy by UVB irradiation. The psoriasis is a complex epidermal disorder characterized by keratinocyte hyperproliferation and abnormal differentiation due to intricate interactions with the immune system. The disease affects 2-4% of the general population and currently has no cure [13, 14]. Specifically, we hypothesize a novel mechanism of stem cell-immune system interaction and predict the chronic disorder as a bimodal switch between a disease phenotypic and a quiescent (seemingly-normal) state. The model hypothesizes a parallel epidermal homeostasis simultaneously maintained by the normal and the psoriatic keratinocytes. The psoriatic homeostasis is caused by permanent perturbations in cell division, apoptosis and differentiation, derived from defective stem cells and their interactions with a weakened immune system. For treatment, the model predicts that to achieve a controlled remission the effective treatment of UVB irradiation must reduce the high-density psoriatic epidermis below a threshold level by activating the apoptosis in stem cells, potentially explaining the chronicity and recurrences of the disorder and providing a guide to design feasible therapeutics.

II. THE MODEL

The model consists of (1) a kinetics model, which tracks the temporal evolution of cell population of keratinocytes at several differentiation stages, and (2) a migration model, which describes motion of individual cells to generate the stratified structure of the epidermis. One can choose the kinetic model as a standalone module to compute the mean-field population dynamics or can integrate the two models to visualize the renewal kinetics and stratification of the tissue.

A. Model of cell population kinetics

Figure 1 illustrates the *central transition pathway* of the epidermis renewal. The pathway considers the population dynamics of six categories of keratinocytes stratified from the stratum basale to the stratum corneum, including progenitors, stem cells (SC) and transit-amplifying (TA) cells in the proliferative compartment, and differentiated cells in the nonproliferative compartment with growth-arrested (GA) cells, spinous (SP) cells, granular cells (GC) and corneocytes (CC). The above classification is primarily based on known histological structure and physiological function of the human epidermis [15]. Growth-arrested cells are precursors for nonproliferating cells. Spinous cells and granular cells are fully differentiated keratinocytes, and the nonnucleated corneocytes represent the end-stage differentiation and eventually desquamate. The central transition pathway incorporates three main cellular processes: (1) proliferation of stem cells and transit-amplifying cells, (2) differentiation including several inter-category cell conversions, and (3) cell loss including apoptosis of nucleated cells and desquamation of the corneocytes.

How stem cells maintain the epidermal homeostasis remains unresolved [16]. However, recent long-term *in vivo* lineage tracing studies on mouse tail tissue by genetic

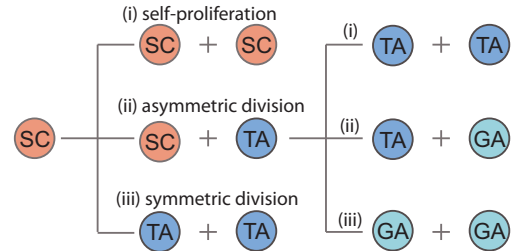


FIG. 2. **Proliferation of stem cell and TA cell.** Both stem cell and TA cell undergo three types of divisions: (i) self-proliferation, (ii) asymmetric division and (iii) symmetric division.

labeling revealed remarkable details about clonal dynamics of epidermal progenitors, suggesting the existence of either single (stem cell alone) or two progenitors (stem cell and committed progenitor) [17–19]. As illustrated in Fig. 2, our model considers a slow cycling stem cell population together with a faster proliferating committed progenitors (or, transit-amplifying cells). A stem cell divides in one of three modes [20–22]: (i) self-proliferation, by which a stem cell divides into two daughter stem cells, (ii) asymmetric division, by which a stem cell divides into a stem cell and a TA cell, or (iii) symmetric division, by which a stem cell divides into two TA cells. Considering a finite availability of stem cell niches [20, 23], we assume a logistic growth of stem cells to limit the stem cell density by a maximal growth capacity, which ensures the system to reach a well-defined steady state (see Ref. [24] for a more general model that guarantees a steady state). Previous models [17, 25] required a precise balance between stem cell self-proliferation and symmetric division and were intolerable to arbitrary perturbations such as population random drift caused by intrinsic stochasticity in the three-mode stem cell division. Similarly, TA cells also divide in one of the three modes of self-proliferation, symmetric and asymmetric division into the GA cells [17, 26, 27]. In addition, a TA cell may resume the stem cell state and a GA cell may resume a TA cell state by backconversions [28].

The rate of progenitor division is often characterized by the cell-cycle time and by the subpopulation of cells that are active to divide (also known as the “growth fraction”). Our mean-field model does not distinguish proliferative propensity in individual cells and therefore parameterizes cell divisions with empirical rate constants that integrate influences of the cell cycle and the growth fraction. Environmental changes regulate the proliferation rate of stem cells. For example, the need of repairing tissue damage promotes stem cell proliferation [19, 21, 29]. Recent study of hair follicles showed that TA cells may signal to stem cells to regulate proliferation [30]. To incorporate this feedback mechanism, we assume an empirical dependence of stem cell division rate constants, γ_1 , k_{1a} and k_{1s} , on the density of TA cells and define:

$$\frac{\gamma_1}{\gamma_{1,h}} = \frac{k_{1a}}{k_{1a,h}} = \frac{k_{1s}}{k_{1s,h}} = \frac{\omega}{1 + (\omega - 1)(p_{ta}/p_{ta,h})^n}, \quad (1)$$

where the subscript h indicates a homeostatic rate constant (see Table III for numerical values), and $\omega \equiv r_{x,\max}/r_{x,h}$ is the ratio of the maximum division rate to the homeostatic rate and is assumed identical for all division processes. ω reflects the maximum increase in the growth fraction and/or decrease in the cell cycle time when stem cell proliferation accelerates. At homeostasis of the normal epidermis, the reported growth fraction varied from 20% to 70% [31, 32]. Study in mice epidermis found more than 10-fold decrease in the cell cycle time from 5–7 days to 11 hours following tissue abrasion [33], whereas no significant change in cell cycle time was found in psoriasis [34, 35]. The exponent n models the sensitivity to the deviation of TA density from the homeostasis. In the limit of a much reduced TA cell density ($p_{ta} \ll p_{ta,h}$), stem cells divide at the maximum rate, $r_{x,\max}$, whereas stem cells divide at a minimal rate when TA cells overpopulate ($p_{ta} \gg p_{ta,h}$). The total stem cell proliferating rate at homeostasis is set about 10^{-2} per day, aligned with 4–6 division events per year [19].

The nonproliferative compartment describes a cascade of differentiations from GA cells to corneocytes. The model also

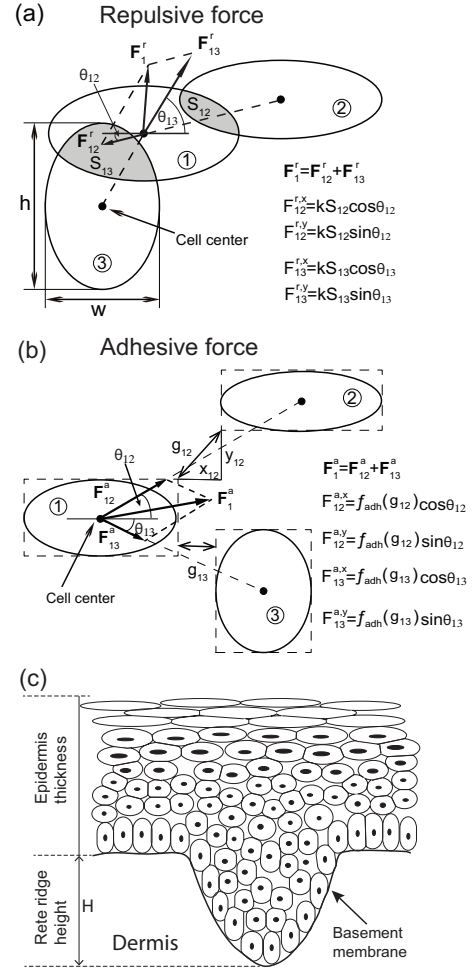


FIG. 3. Mechanics of cell migration. Keratinocytes are geometrically modeled as irrotational ellipsoids with two principal axes staying horizontal or vertical. (a) A repulsive force is determined by an overlap between neighboring cells. The repulsion \mathbf{F}_{12}^r between cells 1 and 2 is proportional to the overlapping area S_{12} approximated by the corresponding overlap rectangle. \mathbf{F}_{13}^r is determined similarly. The net repulsion on cell 1 is a vector sum $\mathbf{F}_1^r = \mathbf{F}_{12}^r + \mathbf{F}_{13}^r$. (b) The adhesive force exists between two adjacent cells. The force \mathbf{F}_{12}^a is related to the distance between cell 1 and cell 2. The direction of \mathbf{F}_{12}^a or \mathbf{F}_{13}^a acting on cell 1 is paralleled to the line (dashed) connecting centers of cell 1 and cell 2. The repulsive force and adhesive force between two overlapped cells are balanced by the force generated by viscosity due to cell motion. Cell motion is only translational without rotation. w and h denote the width and height of a cell. (c) Epidermis thickness, rete ridge height, and undulant basement membrane geometrically configure the epidermis in a 2D projection.

considers an apoptosis process for all nucleated keratinocytes. Early studies suggested that apoptosis was only significant for stem cells and transit-amplifying cells in the proliferative compartment [36]. Recent experiment [37] also showed that apoptosis was evident in the differentiated keratinocytes. The extent of apoptosis is commonly characterized by *apoptotic*

index, which is typically quantified using the TUNEL (transferase-mediated uridine nick end labelling) assay [36]. For a cell type i , the apoptosis index equals the probability that a cell undergoes apoptosis, defined as the ratio of apoptosis rate f_i^{apop} to the total outflux f_i^{out} including rates of apoptosis and transition to the downstream cell category:

$$\text{AI} = \frac{f_i^{\text{apop}}}{f_i^{\text{out}}} = \frac{\beta_i}{\beta_i + k_i}, \quad i = 1, \dots, 5, \quad (2)$$

For stem cells and TA cells, $k_1 = k_{1s}$ and $k_2 = k_{2s}$ are symmetric division rate constants. Experiments often reported global apoptosis indices that did not differentiate apoptotic activities in proliferative and non-proliferative compartments. Apoptotic heterogeneities of cells within a compartment is even less known. Here each cell category is assumed an identical apoptosis index that is used to calculate the apoptosis rate constants β_i 's. Governing system equations (ODEs) are listed in Table I and computation of the model is described in the Supplementary Material (Fig. S1).

B. Model of cell migration

The agent-based migration model describes movement of all keratinocytes in a two-dimensional (cross-sectional) epidermis volume. Keratinocytes once derived from stem cells move outward from the stratum basale to the outermost stratum corneum, to compose a stratified epidermis. The model describes cell mechanics that propels cell movement. An individual cell is subject to three forces: (i) a viscous force due to cell moving in the surrounding environment; (ii) a repulsive force due to cell-cell compression; and (iii) an adhesive force due to interactions among adhesive molecules on cell membranes. Considering the sluggish keratinocyte motion (in a scale of $\mu\text{m/hr}$) in a fluidic environment with a low Reynolds number (i.e., viscosity dominates inertia) [38], the model neglects the acceleration due to inertia. The model also considers keratinocytes as non-chemical tactic cells that do not move by self-propulsion. The force balance for the i th cell is

$$\mu \frac{d\mathbf{x}_i}{dt} + \mathbf{F}_i^r + \mathbf{F}_i^a = 0, \quad (3)$$

where vector \mathbf{x}_i is the cell-center coordinate, and μ is the viscosity coefficient. The first term in Eq. (3) is the viscosity of the epidermis. \mathbf{F}_i^r and \mathbf{F}_i^a are repulsive and adhesive forces between neighboring cells, which are sums of forces derived from all individual pairwise contacts,

$$\mathbf{F}_i^r = \sum_{j \in \mathcal{O}(i)} \mathbf{F}_{ij}^r, \quad \mathbf{F}_i^a = \sum_{j \in \Omega(i)} \mathbf{F}_{ij}^a, \quad (4)$$

where $\mathcal{O}(i)$ and $\Omega(i)$ denote sets of cells overlapping and neighboring with the i th cell and \mathbf{F}_{ij}^r and \mathbf{F}_{ij}^a are force vectors produced onto cell i by interaction (repulsion or adhesion) between cells i and j . By symmetry, $\mathbf{F}_{ij}^r = -\mathbf{F}_{ji}^r$ and $\mathbf{F}_{ij}^a = -\mathbf{F}_{ji}^a$. The model treats individual cells as rigid-body agents and uses the extent of virtual cell overlap to determine the repulsive force [Fig. 3(a)]. Adhesion between two cells is a function of their spatial distance [39, 40] [Fig. 3(b)]. Computation of \mathbf{F}_{ij}^r and \mathbf{F}_{ij}^a is given in the Supplementary Material.

Previous agent-based models [9, 11, 41] treated keratinocytes as identically-sized circles or spheres. However,

cells progressively adopt varied shapes and sizes at different stages of differentiation. Cells in an outer layer generally have more flattened cell body and larger surface area, compared to cells in layers underneath. Tissue location in the body can also influence the cell geometry. For example, compared to the mean basal cell diameter of 6-8 μm at the forearm and hand [42], at unexposed sites in the adult tissue [3], the average cell diameter in the proliferative compartment is about 10 μm whereas the average differentiated cell diameter is about 16 μm . For simplicity, we use ellipsoids to model geometric heterogeneity in cell morphology and size. Cell types are distinguished by the mean major-to-minor axis ratio and the mean nominal size.

The basement membrane of the epidermis is undulant with rete ridges extending downward between the dermal papillae [Fig. 3(c)]. In adult human epidermis, the average rete ridge height is about 40 μm in the adult tissue, and about six rete ridges along 1 mm cross-sectional tissue length were observed [47], which changes with age. The basement membrane is modeled by periodically-repeating Gaussian functions (see the Supplementary Material). Parameters of cell sizes and epidermis thickness are listed in Table II.

III. RESULTS

The model recapitulates two important measures of the epidermis homeostasis: cell counts in different layers and the epidermal turnover times in different compartments.

A. Homeostatic cell density distribution

The mean homeostatic cell densities can be analytically calculated from the ordinary differential equations in Table I as follows (see Table III for definitions of parameters).

$$p_{sc} = p_{sc}^{\max} \left[1 - \frac{1}{\gamma_1} \left(k_{1s} + \beta_1 - \frac{k_{-1}(k_{1a} + 2k_{1s})}{k_{-1} + k_{2s} + \beta_2 - \gamma_2 - \frac{k_{-2}(k_{2a} + 2k_{2s})}{k_{-2} + k_3 + \beta_3}} \right) \right] \quad (5)$$

$$p_{ta} = \frac{k_{1a} + 2k_{1s}}{k_{-1} + k_{2s} + \beta_2 - \gamma_2 - \frac{k_{-2}(k_{2a} + 2k_{2s})}{k_{-2} + k_3 + \beta_3}} p_{sc}, \quad (6)$$

$$p_{ga} = \frac{k_{2a} + 2k_{2s}}{k_{-2} + k_3 + \beta_3} p_{ta}, \quad (7)$$

$$p_{sp} = \frac{k_3}{k_4 + \beta_4} p_{ga}, \quad (8)$$

$$p_{gc} = \frac{k_4}{k_5 + \beta_5} p_{sp}, \quad (9)$$

$$p_{cc} = \frac{k_5}{\alpha} p_{gc}, \quad (10)$$

and the total cell density is given as

$$p_{\text{tot}} = p_{sc} + p_{ta} + p_{ga} + p_{sp} + p_{gc} + p_{cc}. \quad (11)$$

The density of each cell category is proportional to the epidermis capacity of stem cells, p_{sc}^{\max} and the ratio between densities of any pair of cell types is a constant. Therefore,

TABLE I. Kinetic equations for the epidermal renewal and homeostasis

Cell type	Rate equation
Stem cell (SC)	$dp_{sc}/dt = [\gamma_1(1 - p_{sc}/p_{sc}^{\max}) - k_{1s} - \beta_1]p_{sc} + k_{-1}p_{ta}$
Transit-amplifying (TA) cell	$dp_{ta}/dt = (\gamma_2 - k_{2s} - \beta_2 - k_{-1})p_{ta} + (k_{1a} + 2k_{1s})p_{sc} + k_{-2}p_{ga}$
Growth-arrested (GA) cell	$dp_{ga}/dt = (k_{2a} + 2k_{2s})p_{ta} - (k_{-2} + k_3 + \beta_3)p_{ga}$
Spinous cell (SP)	$dp_{sp}/dt = k_3p_{ga} - (k_4 + \beta_4)p_{sp}$
Granular cell (GC)	$dp_{gc}/dt = k_4p_{sp} - (k_5 + \beta_5)p_{gc}$
Corneocytes (CC)	$dp_{cc}/dt = k_5p_{gc} - \alpha p_{cc}$

$p_{sc}, p_{ta}, p_{ga}, p_{sp}, p_{gc}$, and p_{cc} are cell densities.

observed cell density distribution can be used to identify kinetic parameters. The homeostatic TA-cell density is

$$p_{ta,h} = \frac{k_{1a,h} + 2k_{1s,h}}{k_{-1} + k_{2s} + \beta_2 - \gamma_2 - \frac{k_{-2}(k_{2a} + 2k_{2s})}{k_{-2} + k_3 + \beta_3}} p_{sc,h} \quad (12)$$

Kinetic parameters must satisfy two necessary conditions to establish a physiologically proper steady state:

$$\gamma_{1,h} > \beta_1 + k_{1s,h} - \frac{k_{-1}(k_{1a,h} + 2k_{1s,h})}{k_{-1} + k_{2s} + \beta_2 - \gamma_2 - \frac{k_{-2}(k_{2a} + 2k_{2s})}{k_{-2} + k_3 + \beta_3}} \quad (13)$$

$$k_{-1} + k_{2s} + \beta_2 > \gamma_2 + \frac{k_{-2}(k_{2a} + 2k_{2s})}{k_{-2} + k_3 + \beta_3}. \quad (14)$$

Given small backconversion rate (k_{-1} and k_{-2} assumed at 10^{-6} per day, 3-5 orders of magnitude smaller than the stem cell and TA cell proliferating rate constants, Table III), the above conditions simplify to

$$\gamma_{1,h} > k_{1s,h} + \beta_1, \quad \text{and} \quad \gamma_2 < k_{2s} + \beta_2, \quad (15)$$

The first condition ensures the establishment of a viable stem cell population, whereas the second condition prevents an unchecked growth of the epidermis because the proliferation of TA cells is not limited by a maximum capacity in the model. These conditions extend previous treatment that required a precise balance between self-proliferation and symmetric division in progenitor cells when apoptosis was neglected [17, 25]. Apoptosis is a rare event compared to progenitor self-proliferation and symmetric division (e.g., $\beta_1 \ll \gamma_{1,h}$, and $\ll k_{1s,h}$; see Table III) and plays a secondary role in regulating the epidermal homeostasis.

A recent study of progenitors in mice interfollicular epidermis by Mascré et al. [19] suggested that in homeostasis

stem cells proliferate by 4-6 division events per year, 10-20 times slower than proliferation and differentiation (about 1.2 events per week) of committed progenitors (TA cells in our model). This information is reflected such that $k_{1a,h} + 2k_{1s,h}$ is an order of magnitude smaller than $\gamma_2 + 2k_{2s}$. However, considering that TA cells have a much larger population than stem cells ($p_{ta}/p_{sc} \approx 5$ [32]), rates of stem-cell asymmetric and symmetric divisions into TA cells ($k_{1a,h} + 2k_{1s,h}$) must be about 5-fold greater than the difference between TA-cell self-proliferation and symmetric division, i.e., $k_{2s} + \beta_2 - \gamma_2$ based on Eq. (6), assuming backconversion rates (k_{-1} and k_{-2}) are negligible. Therefore, the model predicts that mild perturbations on TA-cell dynamics including proliferation and apoptosis may have substantial effects on the homeostatic keratinocyte population.

The model recapitulates the dynamics and the homeostatic cell density distribution and the epidermal turnover time, in both deterministic and stochastic simulations [Fig. 4(a)]. Starting from an initial stem-cell population, the cell density rapidly increases to reach about 80% of the homeostatic density in the transient phase of the first 100 days and significantly slows down when it approaches the homeostasis. The simulation reached the homeostasis in about 2000 days to a total density at 101684 cells/mm². The transient dynamics is more than an order of magnitude slower than that in the model by Grabe et al. [9, 48], where the authors reported a near 2000-hour transient dynamics from an initial stem cell population to a homeostasis. This discrepancy is caused by a slow stem cell dynamics of 4-6 cell events per year reported recently [19], which also agrees with early-reported cell cycle of 100-200 hrs in a 20% growth fraction in an animal model [49]. Therefore, the stem cell dynamics (Eq. 1) becomes a rate-limiting step to the dynamic establishment of a homeostasis, notably when the system approaches the homeostasis.

Figure 4(b) shows a histogram of the simulated steady-state cell density distribution over different cell types. Stem cells, TA cells and GA cells in stratum basale consist of 22% total cell population, in which proliferating cells accounts for 13.2% total cell population, consistent with the experimental data [32, 50, 51]. Studies by Bergstresser et al. [52] also suggested that 30% of nucleated keratinocytes were in the basal layer where stem cells occupied 10% population [32]. Spinous and granular cells are the majority, consisting of 51.3% total keratinocytes with the population of spinous cells nearly two times that of granular cells, in agreement with a previous prediction by Grabe et al. [9, 48]. Corneocytes consist of 26.6% of the total cell population. Bauer et al. [50] measured a mean nucleated keratinocytes density of 75346 cells/mm² whereas the non-nucleated corneocytes was

TABLE II. Parameters for cell size and the undulant rete ridge

Cell type	w (μm) \times h (μm)	Reference
Stem cell	10×15	[3, 42]
Transit-amplifying cell	10×15	[3, 42]
Growth-arrested cell	12×10	[3, 42]
Spinous cell	12×8	[3, 42]
Granular cell	22.5×4	[3, 42]
Cornified cell	35×1	[43–46]
Rete ridge parameters (see Supplementary Materials):		
$A = 63 \mu\text{m}$, $B = 23 \mu\text{m}$, $\sigma_s = 70 \mu\text{m}$		[47]

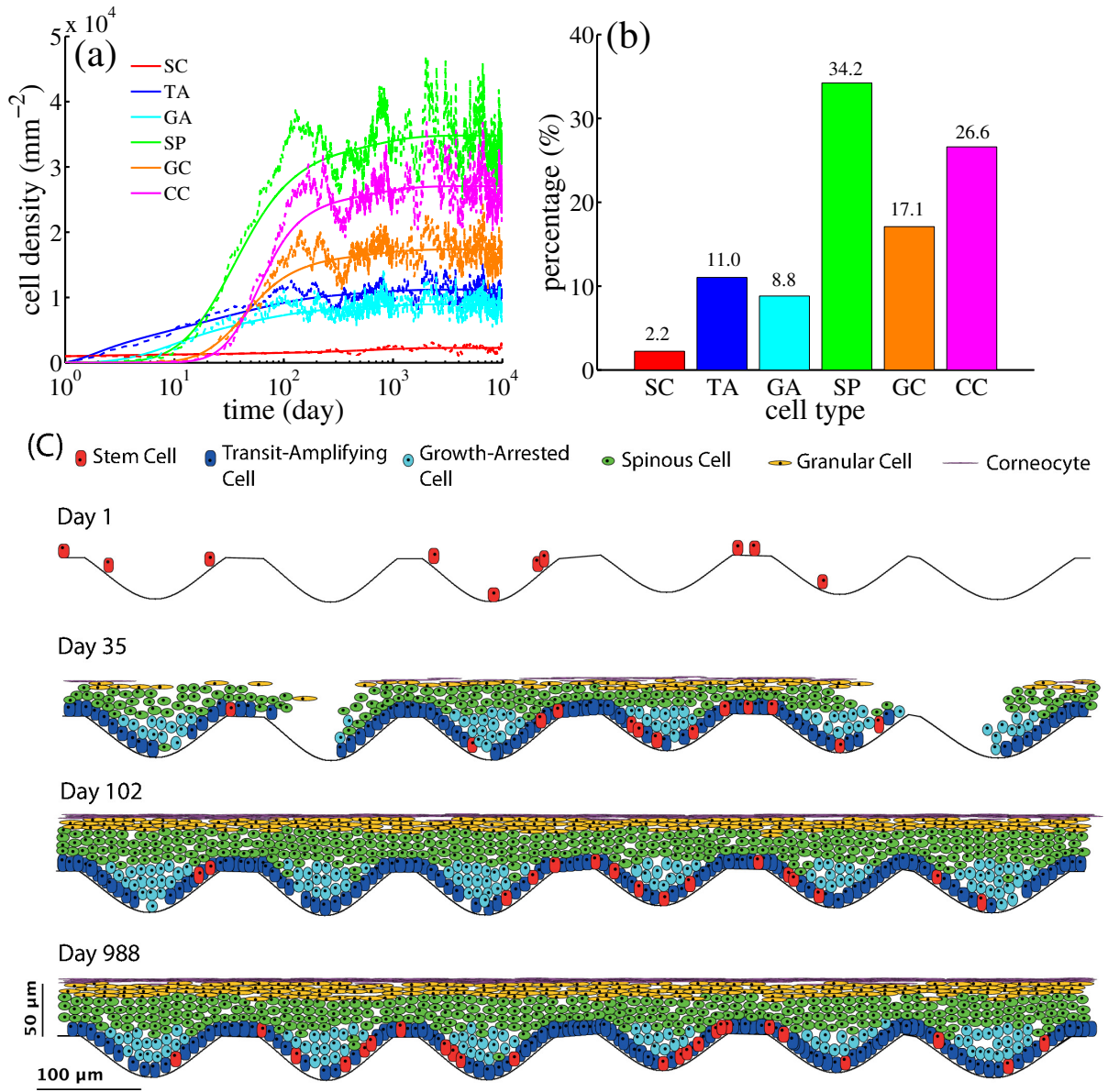


FIG. 4. **Dynamic and homeostatic keratinocytes density distribution.** (a) Temporal evolutions of cell population of different types of keratinocytes by a deterministic simulation (smooth curves) and a stochastic simulation (fluctuated curves). Deterministic simulations started with an initial stem cell density of 1000 mm^{-2} , which corresponds to 10 cells under a skin area of 0.01 mm^{-2} for the stochastic simulation. (b) The histogram of the steady-state cell density distribution. (c) Snapshots at day 1, 35, 102, and 988 of the visualization of the two-dimensional epidermis with a thickness of $10 \mu\text{m}$. Simulation started with stem cells randomly located along the basement membrane (day 1). Parameter values used in simulations are listed in Table III.

estimated to be about 18000 cells/mm^2 , consisting of 19.3% total cell population [51].

Figure 4(c) shows snapshots of temporal evolution of two-dimensional epidermal stratification from an initial group of stem cells distributed along the basement membrane to the homeostasis. We compute the cell population dynamics and the cell migration within an area of 1 mm in length by $10 \mu\text{m}$ in width. The cell density is defined over a surface area number of keratinocytes per mm^2 without explicitly considering the epidermis height. The choice of $10 \mu\text{m}$ (about

the mean cell size) is to visualize a two-dimensional single layer of keratinocytes. The simulated tissue histology shows that the thickness of the nucleated epidermis is about $60 \mu\text{m}$, aligning with observations ranging from $38 \mu\text{m}$ to $77 \mu\text{m}$ with a mean of $60 \mu\text{m}$ in the adult tissue, with little variation across age groups [42, 47, 50]. A movie of the epidermis renewal process of the normal tissue is available at URL: <http://www.picb.ac.cn/stab/epidermal.html>.

B. The epidermal turnover time

Another common measure of epidermis homeostasis is the epidermal turnover time τ . At the tissue level, τ is interpreted as a time required for replacing the entire epidermis with new keratinocytes. The epidermal turnover time varies significantly with age groups, tissue locations and cell densities. In earlier studies, τ has been reported approximately 6-7 weeks in the volar forearm with a nucleated cell density of 44000 mm^{-2} [53, 54]. Based on a more recent count of nucleated cell density of 75346 mm^{-2} on breast skin [50], Hoath and Leahy [51] suggested that τ should be calculated as 59.3 days. Renewal of a specific layer of keratinocytes takes a shorter turnover time. The turnover times of the stratum basale and the differentiated compartment were reported being about 22 and 12 days [54], whereas the stratum corneum has a turnover time that varies from 14 days [54, 55] to about 20 days in young adult [56]. Following the convention [54], we calculate τ as the ratio of total cell density to the rate of cell loss including desquamation and apoptosis, or alternatively, the ratio of total cell density to the rate of cell birth by stem cell and TA cell divisions because cell birth and death rates are balanced at homeostasis:

$$\tau = \frac{p_{\text{tot}}}{r_{\text{growth}}} = \frac{p_{\text{tot}}}{r_{\text{loss}}}, \quad (16)$$

where the rates of cell growth and cell loss are

$$\begin{aligned} r_{\text{growth}} &= [\gamma_1(1 - p_{sc}/p_{sc}^{\text{max}}) + k_{1a} + k_{1s}]p_{sc} \\ &\quad + (\gamma_2 + k_{2a} + k_{2s})p_{ta} \\ r_{\text{loss}} &= \beta_1 p_{sc} + \beta_2 p_{ta} + \beta_3 p_{ga} + \beta_4 p_{sp} + \beta_5 p_{gc} + \alpha p_{cc}. \end{aligned}$$

Analytical solution to τ can be obtained by substituting Eqs. (5)-(10) into the above equation. Apoptosis events represent rare ramifications from the central transition pathway in the normal epidermis renewal. Rate constant of an apoptotic process β_i (10^{-4} - 10^{-5} /day) is much smaller than the differentiation and desquamation rate constants k_i and α (about 10^{-1} /day, see Table III). We can approximate r_{loss} by the rate of desquamation. By also neglecting the backconversions, we have

$$\tau = \tau_{\text{prolif}} + \tau_{\text{diff}} + \tau_{\text{corn}}, \quad (17)$$

where

$$\begin{aligned} \tau_{\text{prolif}} &= \left(\frac{k_{2s} - \gamma_2}{k_{1a} + 2k_{1s}} + 1 \right) \frac{1}{k_{2a} + 2k_{2s}} \\ \tau_{\text{diff}} &= \frac{1}{k_3} + \frac{1}{k_4} + \frac{1}{k_5} \\ \tau_{\text{corn}} &= \frac{1}{\alpha}. \end{aligned} \quad (18)$$

τ is the sum of contributions by sub-compartment turnover times as keratinocytes migrate from the proliferative compartment (τ_{prolif}) through the differentiated compartment (τ_{diff}) and then through the stratum corneum (τ_{corn}). We note that τ is independent of the stem cell self-proliferation γ_1 and the stem cell capacity p_{sc}^{max} . These two parameters determine the steady-state stem cell density p_{sc} . Both cell density and cell growth rate are proportional to p_{sc} , which masks the effect of stem cell self-proliferation dynamics on the turnover times. The turnover time of a single cell category is the inverse of the rate constant for the transit to the next cell category. Therefore, τ can be dominated by a rate-limiting

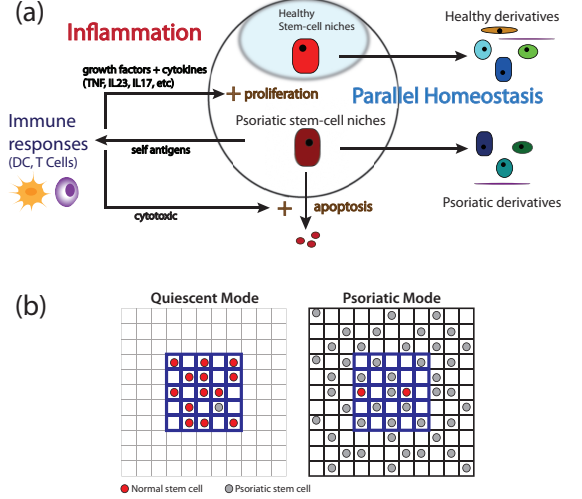


FIG. 5. **Illustration of stem-cell niche environments in the psoriatic tissue.** At the quiescent mode (left panel), healthy stem cells dominate in population, residing in the normal niche repertoire. At the psoriatic mode, psoriatic stem cells dominate in population and the niche repertoire expands to accommodate a larger population of psoriatic stem cells.

step in the cell growth and differentiation cascade. From the calculation by Eq. (16) using parameters in Table III, τ is about 52.5 days, partitioned into 7, 31.5 and 14 days in the proliferative compartment, differentiated compartment and the stratum corneum, respectively, within the wide range of reported adult-tissue measurements between 39 and 75 days [3, 53, 55].

C. Pathogenesis of psoriasis

To investigate an important epidermis disorder, we extend the above model to study the onset and recurrence of psoriasis and its management. Psoriasis, an immune system-mediated chronic skin condition, is characterized by an overproduction of keratinocytes accompanied by inflammation [66], resembling features found in many autoimmune diseases. Here, we focus on studying the most prominent type of the disorder, psoriasis vulgaris, a plaque-formed scaly silvery patch, affecting the majority of psoriasis patients.

Current studies are inconclusive about whether psoriasis (1) arises from genetically hyperproliferative progenitor keratinocytes, or (2) is alternatively induced by a faulty immune system, particularly dendritic cells and T lymphocytes over-response to unresolved self antigens, which in turn produces excessive cytokines (such as $\text{TNF}\alpha$) to promote keratinocyte proliferation, or (3) more likely an intricate interplay between keratinocytes and the immune system [66, 67].

To examine the pathogenesis of psoriasis, we emphasize an interplay between keratinocytes overproduction and responses by the immune system. Our fundamental hypothesis is that a psoriatic epidermis assumes two groups of keratinocytes: normal and psoriatic, maintaining a parallel homeostasis. The

TABLE III. Model parameters

Cell population kinetics model			
Parameter description	Notation (unit)	Value	Source
SC growth capacity	p_{sc}^{\max} (mm ⁻²)	4.50e3	Assumed
Nominal SC self-proliferation rate constant	$\gamma_{1,h}$ (d ⁻¹)	3.30e-3	Estimated
Nominal symmetric SC division rate constant	$k_{1s,h}$ (d ⁻¹)	1.64e-3	[17, 19]
Nominal asymmetric SC division rate constant	$k_{1a,h}$ (d ⁻¹)	1.31e-2	[17, 19]
TA cell self-proliferation rate constant	γ_2 (d ⁻¹)	1.40e-2	[32, 50–52]
TA cell symmetric division rate constant	k_{2s} (d ⁻¹)	1.73e-2	[32, 50–52]
TA cell asymmetric division rate constant	k_{2a} (d ⁻¹)	1.38e-1	[32, 50–52]
GA-to-SP cell differentiation rate constant	k_3 (d ⁻¹)	2.16e-1	[50, 51]
SP-to-GC cell transit rate constant [†]	k_4 (d ⁻¹)	5.56e-2	[50, 51]
GC-to-CC cell transit rate constant [†]	k_5 (d ⁻¹)	1.11e-1	[50, 51]
CC cell desquamation rate constant	α (d ⁻¹)	7.14e-2	[50, 51, 55]
Backconversion rate constant (TA to SC)	k_{-1} (d ⁻¹)	1.00e-6	Assumed
Backconversion rate constant (GA to TA)	k_{-2} (d ⁻¹)	1.00e-6	Assumed
Maximum fold increase of SC proliferation rate	ω	100	[31–33]
Steepness SC proliferation rate regulation by TA cell population	n	3	Assumed
Normal epidermal apoptosis index	AI_h	0.12%	[36, 50, 51]
Psoriatic epidermal apoptosis index	AI_d	0.035%	[36, 50, 51]
Fold change of psoriatic SC proliferation	ρ_{sc}	4	[57]
Fold change of psoriatic TA proliferation	ρ_{ta}	4	[57]
Fold change of psoriatic cell transit rate [†]	ρ_{tr}	5	[58, 59]
Fold change of psoriatic corneocyte desquamation	ρ_{de}	4	[55]
Fold change of psoriatic SC growth capacity	λ	3.5	[60, 61]
Maximum immune killing rate	K_p (mm ⁻² d ⁻¹)	6	Assumed
Immune half-activation psoriatic SC density	K_a (mm ⁻²)	380	Assumed
Cell migration model			
Parameter description	Notation (unit)	Value	Source
Viscosity coefficient	μ (nN·s·μm ⁻¹)	250	[39]
Elasticity constant	k (nN·μm ⁻²)	0.04	Estimated
Adhesion factor of proliferating cells, SC and TA	σ_p (nN)	50	[39, 40]
Adhesion factor of GA and SP and GC	σ_d (nN)	5	[39, 40, 62]
Adhesion factor of CC	σ_c (nN)	0.5	[39, 40, 62]
Mean cell radius	r (μm)	5	Estimated
Time constant of rete ridge remodeling	τ (d)	1000	[63–65]
Maximum rete ridges height of psoriatic epidermis	Y_{\max} (μm)	126	Assumed
Minimal rete ridges height of normal epidermis	Y_{\min} (μm)	40	[47]

[†]In the psoriasis model, due to lack of the granular layer k_4 is the rate constant for SP to CC transition, k_5 is unused, and ρ_{tr} is the fold change in k_3 and k_4 .

psoriatic keratinocytes are derived from a hyperproliferative stem cell population co-residing with the normal stem cells at the basement membrane, which compete for limited stem cell niches ((see Fig. 5 for illustration). This hypothesis can be justified by the existence of intrinsically hyperproliferative stem cells or stem cells that are more responsive to growth stimulants originated from an activated immune system. We modify the above model to describe the competition for niches between the normal and psoriatic stem cells. Dynamics of psoriatic TA and nonproliferative cells are governed by rate equations as in Table I for the normal keratinocytes, however,

with different parameter values to generate known phenotypes in psoriatic plaques, with an exception of granular cells that are missing in psoriasis. The dynamics of psoriatic stem cells in our model is similar to the model of spruce budworm outbreak by Ludwig et al. [68], which models a single-species population growth under predation.

$$\frac{dp_{sc}}{dt} = \left[\gamma_1 \left(1 - \frac{p_{sc} + \tilde{p}_{sc}/\lambda}{p_{sc}^{\max}} \right) - k_{1s} - \beta_1 \right] p_{sc} + k_{-1} p_{ta} \quad (19)$$

TABLE IV. Cell density distribution (mm^{-2}) and turnover times (day)*

	Healthy tissue	Psoriasis [†]	Non-symptom [†]
SC	2268	362+6459	2232+124
TA	11219	77+32098	10715+618
GA	8964	61+20536	8562+395
SP	34799	238+79788	33236+1536
GC	17379	119+0	16598+0
CC	27055	185+77633	25840+1495
Total	101684	1042+216514	97183+4168
$\tau = \tau_{\text{prolif}} + \tau_{\text{diff}} + \tau_{\text{corn}}$	52.5=7.0+31.5+14.0	9.8=1.8+4.5+3.5	44.5=6.0+26.5+12.0

[†]Normal+Psoriatic ($p_x + \tilde{p}_x$).

*Results are generated using parameters in Table III.

$$\frac{d\tilde{p}_{sc}}{dt} = \left[\rho_{sc}\gamma_{1,h} \left(1 - \frac{p_{sc} + \tilde{p}_{sc}}{\lambda p_{sc}^{\max}} \right) - \rho_{sc}k_{1s,h} - \tilde{\beta}_1 \right] \tilde{p}_{sc} - f(\tilde{p}_{sc}) + \tilde{k}_{-1}\tilde{p}_{ta} \quad (20)$$

$$f(\tilde{p}_{sc}) = \frac{K_p \tilde{p}_{sc}^2}{K_a^2 + \tilde{p}_{sc}^2}. \quad (21)$$

The psoriatic tissue activates the immune system to combat disease cells. We assume that repertoires for normal p_{sc} and psoriatic \tilde{p}_{sc} stem cells are both limited by available niche environment and psoriatic stem cells can acquire a larger growth capacity. Parameter λ (> 1) accounts for the fold increase in the growth capacity accessible to stem cells. The density of normal stem cells remains limited by p_{sc}^{\max} , which is invaded by a fraction ($1/\lambda$) of psoriatic stem cells. Equation (21) models the immune activities triggered by psoriatic stem cells. An activated immune system induces apoptosis of psoriatic stem cells. The activity of the immune system (the killing rate, $f(\tilde{p}_{sc})$) is directly regulated by the psoriatic stem cell density, under the assumption that the immune system is activated in a faster time scale than the tissue growth. The immune response is significantly activated when \tilde{p}_{sc} exceeds a threshold parameterized by K_a and is saturated at the maximum rate K_p at $\tilde{p}_{sc} \gg K_a$ when the psoriatic stem-cell population overwhelms that of cytotoxic T cells. This approach hypothesizes that the immune system combats disease stem cells, but does not exclude the commonly-believed role by the immune system of inducing keratinocyte overproduction, even though the model does not explicitly couple the immune system to stem-cell proliferation.

Proliferation rate constants γ_1 , k_{1s} and k_{1a} for the normal stem cells are regulated by the total TA cells, $p_{ta} + \tilde{p}_{ta}$, similar to Eq. (1):

$$\frac{\gamma_1}{\gamma_{1,h}} = \frac{k_{1a}}{k_{1a,h}} = \frac{k_{1s}}{k_{1s,h}} = \frac{\omega}{1 + (\omega - 1)[(p_{ta} + \tilde{p}_{ta})/p_{ta,h}]^n}. \quad (22)$$

In comparison, we assume that psoriatic stem cells are not subject to regulation by the TA cell population and proliferate with rates ρ_{sc} -fold higher than the homeostatic rate constants ($\gamma_{1,h}$, $k_{1a,h}$ and $k_{1s,h}$) of normal stem cells. We assume that the immune response substantially switches on when the psoriatic stem cell population reaches 10% of stem cell population in the normal tissue. This assumption is used to parameterize the steepest change in the removal rate $f(\tilde{p}_{sc})$ in response to \tilde{p}_{sc} , which sets the half-activation density at

$K_a = \sqrt{3}p_{sc,h}/10$. The model does not consider immune responses against cells derived from psoriatic stem cells by observing that reduction in stem cell population results in a subsequent reduction in the derived keratinocyte population.

Despite its mechanistic uncertainties, psoriasis plaques have well-defined tissue-level phenotypes, making it a good candidate for study by a predictive model. Depending on its severity a plaque exhibits 2-5 times increase in the total cell density [57, 58, 69] with a relatively higher growth in the proliferative compartment compared to the nonproliferative compartment [60, 61]. A disordered tissue usually loses the granular layer due to abnormal differentiation and contains a subset of nucleated corneocytes. A psoriatic plaque also has a turnover time several fold faster [55, 70]. More specifically, studies found in the cell kinetics of psoriasis (i) significant increase of cell cycle marker Ki-67 in psoriatic tissue without much change in cell cycle time [35, 71], suggesting a substantial increase in growth fraction; (ii) transit time of keratinocytes through differentiated compartment is shortened to 48 hrs from 240-330 hrs, 5-7 times faster than in the normal tissue [59]; (iii) transit time through the corneum is also shortened from 14 days to 2 days [55]. These factors together result in a decrease in the epidermis turnover time [Eq. (17)]. In addition, the cell apoptotic index decreases nearly four fold from 0.12% to 0.035% [36], making a further contribution to keratinocytes overproduction. Table III lists parameter values based on the above observations, where coefficients ρ_{ta} , ρ_{tr} and ρ_{de} are fold changes over rate constants in normal kinetics of TA-cell proliferating (γ_2 , k_{2a} and k_{2s}), transit in the nonproliferative compartment (k_3 and k_4) and desquamation (α), respectively. Like variations in normal tissues, severity and phenotype of psoriasis vary widely across individuals and disease subtypes and therefore for any specific condition or study the model should be parameterized accordingly.

As the main result, the model predicts two interconverting homeostatic modes of the psoriatic tissue (see the Appendix for analytical details): (1) a *disease* state, which generates psoriasis phenotypes of keratinocytes overproduction and a shortened epidermal turnover time when psoriatic stem cells outcompete normal stem cells for available niches and overwhelm the immune system; and (2) a *quiescent* state, which predicts a coexistence of a small number of psoriatic cells with a dominant population of normal keratinocytes when the immune system keeps the psoriatic stem cell population low. The quiescent mode with remanent psoriatic

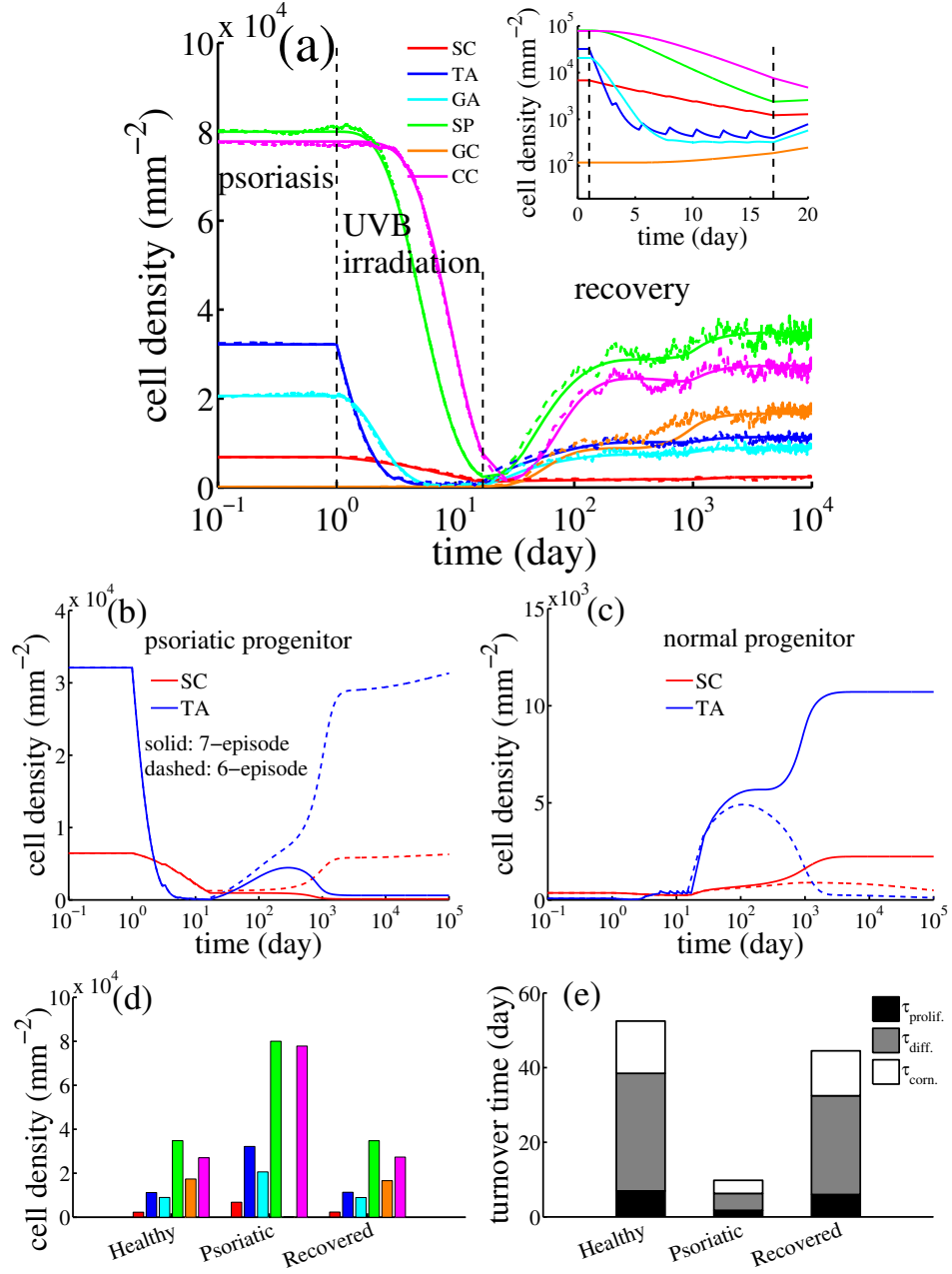


FIG. 6. **Psoriasis and its management by phototherapy.** (a) Three dynamical phases of cell densities from psoriasis, the UVB treatment and recovery. Trajectories are combined populations of psoriatic and normal cells. Both stochastic and deterministic trajectories are shown. The stochastic simulation was conducted in an area of 0.1 mm^{-2} . Inset: zoomed details of the UVB irradiation phase (from day 1 to day 17). Psoriatic (b) and normal (c) stem cell and TA cell densities before and after 6- or 7-episode treatment. The treatment started at time day 1. Each simulated UVB irradiation episode induces 60000-fold increases in apoptosis rate constants for stem cells and TA cells and lasts for 48 hours. The time interval between two consecutive episodes is 56 hours (48-hr irradiation + 8-hr resting). (d) and (e) Homeostatic cell density distributions and the epidermal turnover times for healthy, psoriatic and recovered tissues. Notice that the granular layer is missing in the psoriatic tissue.

stem cells is a symptomless state for a psoriasis susceptible tissue and may relapse into the disease state given favorable conditions. On the other hand, the disease state may be reverted back to the quiescent state by a properly designed treatment.

The model is parameterized (Table III) to produce a specific psoriasis phenotype, in which the total cell density reaches 217000 mm^{-2} at homeostasis, more than two times the normal epidermis (101600 mm^{-2}), with the pathological keratinocytes consisting of 99.5% of the total population.

The relative growth of the proliferative compartment over the nonproliferative compartment is about 3 vs. 2 times the normal densities (Table IV). The epidermal turnover time is shortened more than 5 times from 52.5 days to 9.8 days.

The psoriatic epidermis may retreat to the “quiescent” state and achieve a remission provided that the psoriatic stem cell density can be managed below a threshold value (see the Appendix). Narrow-band 311 nm controlled UVB irradiation is known as an effective treatment for managing psoriasis [72]. For example, a recent study by Weatherhead et al. [58] applied sequential episodes of 0.75-3 MEDs (minimal erythral dose) UVB irradiation to achieve plaques remission by inducing strong apoptosis of proliferative cells. Figure 6(a) shows a model simulation of a psoriasis remission after a simulated sequence of 7-episode UVB irradiations. Each UVB irradiation episode is simulated by increasing apoptosis rate constants 60000 fold indiscriminately for normal and psoriatic stem cells and TA cells for 48 hours followed by a 8-hour resting interval before starting the next episode. The entire treatment lasts 16 days. Model simulations unveil an intriguing interplay between dynamics of psoriatic and normal cells. Upon the initiation of irradiation, the total cell population first declines due to the UVB-induced apoptosis in stem cells and TA cells. Each episode of UVB irradiation induced apoptosis in about 22% stem cells in the pre-episode population [see Fig. 6(a) inset]. The population of TA cells declined more substantially due to combined effects of increased apoptosis and reduced stem-cell symmetric and asymmetric divisions. A mild rebound of cell densities happens in each resting interval because of a continuing hyper-proliferation of psoriatic stem cells and TA cells. At the end of the treatment, the total keratinocyte density dramatically drops more than 95% from 217000 to 12100 mm^{-2} , with normal and psoriatic stem cells respectively reduced to 260 and 960 mm^{-2} . Post-treatment stem-cell population continues to decline to the “quiescent” steady state due to a relatively stronger immune response [Fig. 6(b) and Fig. S3(c) and related text in the Supplementary Materials], which later brings down the psoriatic cell density to a minimum (less than 0.5% of the total cell density, Table IV). The granular cells become visible during the recovery. The last phase indicates a recovery of keratinocytes derived from the normal stem cells that reclaim their niche repertoire by a slower kinetics [Fig. 6(c)]. The downstream differentiated cells follow similar dynamics of remission. Simulated dynamics is similar if the model considers UVB-induced apoptosis in all nucleated cells [results not shown].

A treatment with less UVB irradiation episodes and/or inadequate intensity may fail to clear a psoriatic plaque, which eventually returns to the disease state once the treatment stops due to an insufficient loss in psoriatic stem cells. Figure 6(b) and (c) show that after a 6-episode UVB irradiation treatment, the psoriatic stem cell and TA cell populations bounce back to the disease state after terminating the treatment. The total cell density drops to 18600 mm^{-2} at the end of the 6th episode with the normal and psoriatic stem cell densities as 247 and 1263 mm^{-2} , respectively. Interestingly, the end-treatment normal stem-cell count is slightly less than that from 7-episode treatment, implying that increased normal stem cell proliferation rate due to loss of TA cells well below the healthy level offsets the cell loss caused by apoptosis. Shortly after the treatment stopped, both psoriatic and normal stem cells and TA cells started slow

increases, but later the density of psoriatic cells [Fig. 6(b)] rapidly expands and outcompetes the normal cells [Fig. 6(c)] that retreat from a maximum to the steady state at a lower level. During the entire course of the treatment the cytotoxic rate remains below the growth rate of psoriatic stem cells, giving no chance for the immune system to effectively reduce the psoriatic stem cell population (see Fig. S3(d) in the Supplementary Materials).

Histograms in Fig. 6(d) and (e) show that a well-designed treatment can manage the psoriatic tissue to the quiescent state that is almost phenotypically indistinguishable from the healthy tissue in cell density distribution and the turnover time. Histologically, psoriasis causes thickening in the stratum corneum and the differentiated layer as well as an expanded proliferating compartment with more protruding rete ridges [73]. A dynamic model of rete ridge remodeling, simulation snapshots of the homeostatic psoriatic epidermis, tissue under treatment and recovered tissue can be found in the Supplementary Material (Fig. S3-S4). Movies of simulations (normal and psoriatic tissues) are provided at URL: <http://www.picb.ac.cn/stab/epidermal.html>.

IV. DISCUSSION

We presented a hybrid model that simulates and visualizes spatiotemporal dynamics of the epidermal homeostasis. The model represents an efficient approach that separates the computation of cell kinetics from that of an agent-based cell migration. Compared to previous agent-based models [8, 9, 11, 12], our population kinetics model describes cell proliferation, differentiation and cell death as empirical rate processes and can be simulated by integrating the governing ordinary differential equations (Table I) or the master equations by a kinetic Monte Carlo algorithm. The cell population kinetics model can be combined with a two-dimensional cell migration model to visualize dynamics of epidermis renewal and stratification. The model reproduces observed characteristics of the normal epidermis. Model analysis and simulations show that balancing cell production and cell loss in each subcompartment is critical to establishing and maintaining a proper epidermis homeostasis (Fig. 4).

The current model has some addressable limitations: (i) The cell population kinetics does not explicitly incorporate specific intracellular and extracellular factors that affect the dynamics and steady state of the epidermis homeostasis. However, physiological and physical factors including age and UV irradiation as well as many commonly investigated signaling molecules can be coarsely coupled to model parameters such as proliferation and differentiation rate constants and morphology of keratinocytes and the epidermis. (ii) We neglected the effects by backconversions from TA cells to stem cells and from differentiated cells to TA cells by assuming their minimal impact. These processes could be worth a close examination as suggested in a recent theoretical study [74] that showed rare backward transitions may cause catastrophic outcome such as a cancerous growth. (iii) Technically, as intensive modeling and computation is made possible by high-performance hardware [75, 76], our two-dimensional cross-sectional model can be extended to simulate a more realistic three-dimensional epidermis even though we expect that the qualitative results obtained from the 2D model remain valid in a 3D model.

As an important application, a non-trivial extension to the above model allows us to investigate the pathogenesis of psoriasis, an immune-mediated skin disorder. Genetic origins of psoriasis have been recently explored by an increasing number of genome-wide association studies that identified a multitude of psoriasis susceptibility loci [77–80]. Many psoriasis-associated loci are connected to genes in the immune system (e.g., MHC class I molecules) and proteins expressed in keratinocytes, suggesting a complex nature of the disease [81]. However, the mechanistic epidermis-immune system interactions implicated by these loci are yet to be resolved.

In this study, we propose an alternative hypothesis of interactions between the immune system and keratinocytes, in which the disordered epidermis maintains a parallel homeostasis of both normal and psoriatic keratinocytes, derived from respective stem cell populations. We examine this hypothesis in an extended model and demonstrate that treatment by UVB irradiation with consecutive episodes can potentially manage the disease and achieve a remission of the psoriatic phenotype.

Psoriasis has recently been studied by agent-based models [48, 58]. The model by Grabe and Neuber [48] was able to generate the psoriasis phenotype of an increased cell density and a shortened epidermal turnover time, by adjusting the fractional time of TA cell proliferation. This parameter characterizes the amount of time for proliferation during a constant life time of a TA cell, which in our model is embedded in the TA cell self-proliferation rate constant γ_2 . Increasing γ_2 and keeping symmetric division rate constant k_{2s} unchanged (equivalent to keeping a constant TA cell life time) does increase TA cell population (Eq. 6). To obtain a relative growth of the proliferating compartment, rate constants for cell differentiation must have relatively higher increases than γ_2 , which was achieved by modulating Ca^{2+} gradient in the Grabe and Neuber model. The model however did not propose possible management that can target the hypothesized mechanism. For example, it is not obvious how apoptosis induced by episodes of UVB irradiation can attain a remission via recovering the normal TA cell proliferating time. Weatherhead et al. [58] developed a model to simulate UVB-induced apoptosis in stem cells and TA cells, which was able to demonstrate a psoriasis remission after a few episodes of UVB irradiation. The model assumed a constant pool of stem cells that derived TA cells by asymmetric division and the UVB-induced apoptotic hyperproliferative stem cells were replaced with normal stem cells by symmetric divisions. This model assumption consequently led to a permanent reduction in cell density after each UVB irradiation treatment and therefore did not explain relapses of psoriatic phenotypes once an ineffective treatment ends or recurrence of the disorder.

Interactions between the immune system and keratinocytes considered in our model can serve as a conceptual basis for interpreting the pathogenesis of psoriasis. Especially, we showed that the act of the immune system cytotoxicity against psoriatic keratinocytes plays a pivotal role in the onset, remission and recurrence of the disease phenotype. The most common paradigm considers that faulty immune responses triggered by unknown self antigens or pathogens (introduced by injuries or trauma, known as Koebner phenomenon) produce cytokines and growth factors that promote keratinocyte hyperproliferation, immature differentiation and skin inflammation, establishing the psoriasis phenotype. Drugs that inhibit T cell activity and cytokine productions

do improve psoriatic conditions [82]. In contrast, our model demonstrates that a psoriasis lesion develops when the immune system is genuinely weakened or locally overwhelmed by a large population of psoriatic keratinocytes, staging up a chronic condition. This prediction may explain high occurrence and increasing severity of psoriasis in HIV-infected, especially late-stage AIDS patients with substantially compromised immune systems when CD4+ and naive CD8+ T cell counts substantially decrease [83, 84]. Furthermore, the onset age of psoriasis has been known to have two separate populations, type I (early onset in patients younger than 40 with a peak at age 20) and type II (late onset after age 40 with a peak at about 60) [85]. Our model speculates that a vigorous immune system at a younger age can stimulate a strong hyperproliferation (a large ρ_{sc}) in a psoriatic epidermis and causes manifestation of plaque phenotypes. One the other hand, a weak immune system (a small k_p) at an older age can also have an equivalent effect.

The model prediction provides an alternative (a less explained) perspective of the pathogenesis of psoriasis, suggesting that psoriasis is a parallel epidermal homeostasis due to heterogeneity in stem cell clones, and that the immune system as a double-edged sword plays two essential however opposing roles: (i) Cytotoxic (CD8+) T cells recruited to the epidermis induce apoptosis in psoriatic stem cells, which is implicated by studies that demonstrated CD8+ T cell (especially, CD45RO+ memory subtype) count and cytotoxic proteins including perforin and granzyme B substantially increase in psoriatic lesions [83]; and (ii) Immune activities in the meantime promote progenitor keratinocytes proliferation by producing a multitude of cytokines and growth factors (TNF, IFN- α , IFN- γ , IL-17, IL-22, IL-23, etc.). Balance between the two acts determines the outcome of the disease. Our model predicts that the psoriasis-susceptible tissue is a bimodal system and can switch between a non-symptom state and a phenotypical state, potentially explaining the recurring nature of the disorder and suggesting the feasibility of disease management by an effective treatment. This perspective and the model could be in general applicable to other autoimmune diseases in regenerative tissues.

We showed in UVB phototherapy simulation that psoriasis plaque clearance can be attained by inducing strong apoptosis in keratinocytes. The model only considered UVB-induced apoptosis in keratinocytes. UVB irradiation may promote proliferation and differentiation in skin cells [86, 87] or may alter immune responses. These effects could be incorporated and be examined in the model. For example, as suggested in Eq. (20), rebalance in self-proliferation $\gamma_{1,h}$ and symmetric division $k_{1s,h}$ and change in immune activities $f(\bar{p}_{sc})$ may affect the population of psoriatic stem cells and thus the therapeutic outcome. Experiments did not demonstrate whether the UVB irradiation causes non-apoptotic cell death that was not reflected by an apoptosis marker [58]. Regardless the actual mechanism, induced cell deaths will result in a shift of the stem cell density from the disease state to the quiescent state across the phase boundary, an important parameter that determines the design of a phototherapy regimen, including irradiation dosage in each treatment episode, the number of episodes and the time interval between consecutive episodes.

The model also suggests the limitation of UVB irradiation or similar treatments that attempt to achieve plaque remission by killing keratinocytes below a critical threshold. First, psoriasis plaques may recur under a temporally-weakened immune system or a transient burst of

cell proliferation caused by conditions such as wound healing. Second, the psoriatic severity may be worsened under a genuinely weak immune system (with a low K_p and/or a high threshold K_a), in which the disease phenotype persists and cannot be adequately reverted by simple reduction in psoriatic stem cells because the system does not possess a quiescent state [region I in Fig. 7(b)]. In the latter case, other treatment options such as cytokine-targeting biologic and small-molecule drugs should be considered to at least shift the disorder to the bimodal region where phototherapy becomes effective. However, we note that phototherapy may be effective through alternatively mechanisms other than induction of apoptosis [88, 89], by which it alone may switch a plaque from persistent disorder (region I) to bimodal (region II) or symptomless (region III) as in Fig. 7(b).

Further insight from the model is that the bimodal psoriasis exhibits hysteresis, by which a mode of the epidermis, psoriatic or quiescent, once reached under a favorable condition, will tend to be relatively stable. For example, a symptomless epidermis as illustrated in Fig. 7(b) may switch to the disease state when K_p is reduced beyond its lower threshold because of weakening in the immune system. However, restrengthening the immune system to revert the disease state back to the quiescent mode requires elevating K_p in the model beyond the upper threshold, implying that the disease is resistant to mild natural or induced perturbations.

One definitive experimental test of our model hypothesis should aim at simultaneously tracing clones of psoriatic and normal stem cell lineages. Because of recent advancement in techniques, studies of epidermal stem cells become central to the understanding of the epidermal homeostasis. Especially, the emerging powerful *in vivo* lineage tracing technology allows dynamic monitoring of stem cells and progenitors clone formation and differentiation and can achieve multicolor simultaneous tracing of separate clones [27]. The technique has already been pioneered to study progenitor fates in normal skin tissue [17] and benign epidermal tumors [90] and can be potentially applicable to identify the coexistence of normal and psoriatic progenitors in psoriasis. One potential challenge is that in either quiescent or disease state one type of stem cells is in a small population (about a 1:20 ratio, according to Table IV), making it difficult for differential labeling. Alternatively, an experiment may tend to identify and isolate the two competing effects by the immune system on the epidermis: (1) apoptosis in epidermal progenitors by T-cell cytotoxic activities and (2) hyperproliferation due to elevated cytokines and growth factors.

Appendix A: Analytical details of the psoriasis model

Psoriasis as a bimodal switch — To illustrate the principle and simplify the analysis, we only present a two-dimensional model that describes dynamic interactions between normal and psoriatic stem cells. The complete model that produced the results (Fig.6) is more complex and of a higher dimension because of the feedback regulation by TA cell population on the normal stem cell proliferation (Eq. 22), requiring analyzing the dynamics of normal and psoriatic TA cells together. Again, for convenience in analysis, we neglect the influences of backconversions and apoptosis. This simplification allows us to show insights of the model

behaviors without much mathematical complication. We work with normalized quantities:

$$x = \tilde{p}_{sc}/K_a, \quad y = p_{sc}/K_a, \quad y^{\max} = p_{sc}^{\max}/K_a, \quad k_p = K_p/K_a.$$

Ratios between the normal stem-cell proliferation rate constants remain constant despite their dynamic modulations by the TA cell population (Eq. 1), i.e., $k_{1s}/\gamma_1 = k_{1s,h}/\gamma_{1,h}$. Ignoring the trivial steady states of zero density ($x = 0$, and/or $y = 0$), based on Eqs. (19-21) we have the steady-state equations for stem cell densities as

$$w \left(1 - \frac{x}{u} \right) - \frac{x}{1 + x^2} = 0, \quad (A1)$$

$$y = \frac{u - x}{\lambda}, \quad (A2)$$

where

$$w = \frac{\rho_{sc}}{k_p} (1 - 1/\lambda) (\gamma_{1,h} - k_{1s,h}),$$

$$u = \lambda y^{\max} (1 - k_{1s,h}/\gamma_{1,h}).$$

Eq. (A1) can solve for one or three steady-state psoriatic stem cell densities, only depending on choices of two parameters, w and u , which is illustrated in Fig. 7(a).

To study plaque remission and relapse, we are interested in the region where the system has two stable steady states, “quiescent” and “disease”, and one unstable “transition” steady state. This scenario is illustrated in Fig. 7(a) with three intersections between the line $w(1 - x/u)$ and the nonparametric curve $x/(1 + x^2)$. Determination of the stability of these fixed points requires analysis similar to the spruce budworm model by Ludwig et al. [68]. Figure 7(a) shows that the “quiescent” state is more sensitive to w , whereas the “disease” state is determined by both u and w . This observation provides a guideline to parameterize the model to attain appropriate psoriatic phenotypes by identifying disease-related parameters ρ_{sc} , λ and k_p . The ratio ρ_{sc}/k_p emerges as the key parameter that characterizes the interplay between proliferation of keratinocytes and activity of the immune system (magnitude K_p and threshold K_a), playing a critical role in the interpretation of the pathogenesis of psoriasis.

Bifurcation diagrams in Fig. 7(b) of steady-state stem cell densities shows three classes of behaviors as ρ_{sc}/k_p varies. A small population of psoriatic stem cells survive in the “quiescent” state ($\rho_{sc}/k_p < 159$ day) under a vigorous cytotoxic activity (a large k_p , i.e., a low threshold K_a and/or a high magnitude K_p) and/or a moderate stem-cell proliferation (a small ρ_{sc}). In contrast, a weak immune system (a small k_p , i.e., a high threshold K_a and/or a low magnitude K_p) cannot adequately counterbalance the psoriatic hyperproliferation (a large ρ_{sc}) and thus the epidermis assumes a persistent “disease” state ($\rho_{sc}/k_p > 440$ day). A bimodal system with an intermediate ρ_{sc}/k_p has a potential to switch between the quiescent and disease modes when conditions change. Figure 7(c) shows a two-dimensional phase plane of normal and psoriatic stem-cell densities. Starting from initial stem cell densities, located inside region I or II, a temporal trajectory will be attracted to the quiescent or the disease state, respectively. Those starting on the boundary of the two regions will in theory converge to the transition state, which is unsustainable because slight perturbations will dislocate a trajectory into either region I or II.

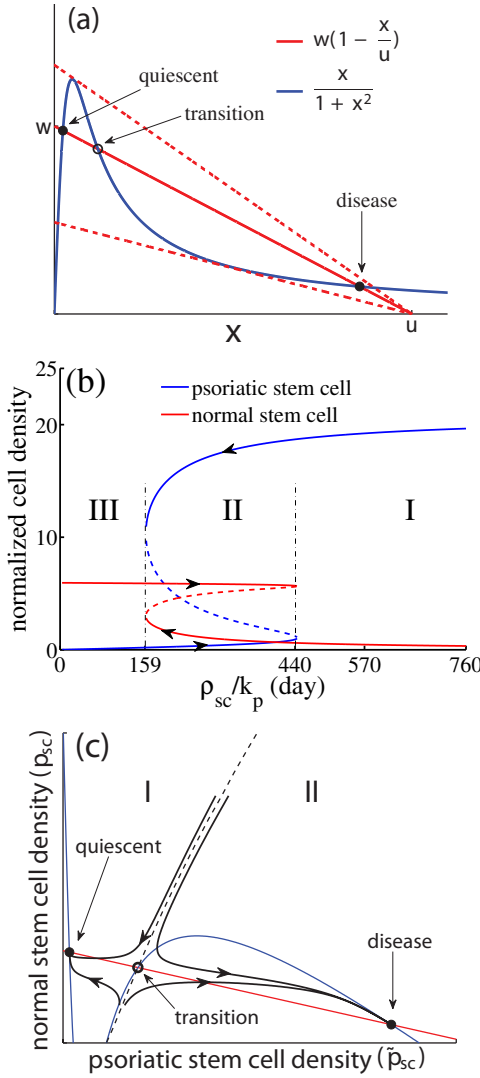


FIG. 7. **Steady states of the psoriasis model.** (a) Intersections of the two functions give the steady states (Eq. A1) and can be modulated with w by changing K_p within the range of two bifurcation points (indicated by dashed lines). The “quiescent” and “disease” states (filled circles) are stable steady states. The “transition” state (empty circle) is unstable (i.e., arbitrarily small perturbations deviate the system away from it). (b) Bifurcation diagram under varying ratio ρ_{sc}/k_p with three regions: (I) persistent disorder, (II) bimodal, and (III) symptomless. (c) Trajectories from basins of attraction: I and II, separated by the boundary (dashed line), converging to the quiescent and disease states, respectively. Blue and red curves are nullclines (Eqs. A1 and A2). Parameter values used for the simulation are listed in Table III.

Cell density and turnover time — Below, we provide equations for homeostatic cell densities and the turnover time in the psoriatic model. As shorthands, we define

$$g = \frac{k_{1a} + 2k_{1s}}{k_{2s} - \gamma_2}, \quad g_h = \frac{k_{1a,h} + 2k_{1s,h}}{k_{2s} - \gamma_2},$$

The ratio $\xi = g/g_h$ is a function of the steady-state TA cell

population ($p_{ta} + \tilde{p}_{ta}$) by Eq. (22). The total steady-state cell density is given as

$$p_{tot} = p_{sc} (1 + \xi g_h W) + \tilde{p}_{sc} \left(1 + \frac{\rho_{sc}}{\rho_{ta}} g_h \tilde{W} \right),$$

where

$$W = 1 + (k_{2a} + 2k_{2s}) \left(\frac{1}{k_3} + \frac{1}{k_4} + \frac{1}{k_5} + \frac{1}{\alpha} \right),$$

$$\tilde{W} = 1 + (k_{2a} + 2k_{2s}) \left(\frac{1}{\rho_{tr} k_3} + \frac{1}{\rho_{tr} k_4} + \frac{1}{\rho_{de} \alpha} \right) \rho_{ta}.$$

Notice the lack of GC layer in the psoriatic cell population. The proliferative and differentiated cell populations are

$$p_{prolif} = p_{sc} (1 + \xi g_h) + \left(1 + \frac{\rho_{sc}}{\rho_{ta}} g_h \right) \tilde{p}_{sc}$$

$$p_{diff} = g_h (k_{2a} + 2k_{2s}) \left(p_{sc} \xi + \frac{\rho_{sc}}{\rho_{tr}} \tilde{p}_{sc} \right) \left(\frac{1}{k_3} + \frac{1}{k_4} \right) + p_{sc} \xi g_h \frac{k_{2a} + 2k_{2s}}{k_5}.$$

Corneocytes are not included in the differentiated compartment. By comparison, the cell densities in the healthy tissue are

$$p_{prolif,h} = p_{sc,h} (1 + g_h),$$

$$p_{diff,h} = g_h (k_{2a} + 2k_{2s}) p_{sc,h} \left(\frac{1}{k_3} + \frac{1}{k_4} + \frac{1}{k_5} \right).$$

We can calculate the growth of the proliferative compartment relative to that of the nonproliferative compartment as

$$\frac{p_{prolif}/p_{prolif,h}}{p_{diff}/p_{diff,h}} = \frac{p_{sc} (1 + \xi g_h) + \left(1 + \frac{\rho_{sc}}{\rho_{ta}} g_h \right) \tilde{p}_{sc}}{(1 + g_h)} \times \frac{\frac{1}{k_3} + \frac{1}{k_4} + \frac{1}{k_5}}{\left(p_{sc} \xi + \frac{\rho_{sc}}{\rho_{tr}} \tilde{p}_{sc} \right) \left(\frac{1}{k_3} + \frac{1}{k_4} \right) + p_{sc} \xi \frac{1}{k_5}} > \frac{p_{sc} (1 + \xi g_h) + \left(1 + \frac{\rho_{sc}}{\rho_{ta}} g_h \right) \tilde{p}_{sc}}{(1 + g_h) \left(p_{sc} \xi + \frac{\rho_{sc}}{\rho_{tr}} \tilde{p}_{sc} \right)}.$$

A relative increase in the proliferative population requires the above ratio to be greater than 1. In psoriasis, $\xi < 1$, reflecting a decreased proliferation rate in the cohabitating normal stem cell population due to a much elevated TA cell population. It is unclear whether stem cells and TA cells have differential increases in proliferation rates. For the lack of information, we assume $\rho_{sc}/\rho_{ta} \approx 1$. Therefore, $\rho_{tr} > \rho_{sc}$ becomes a sufficient (but not a necessary) condition to produce a relative increase in the proliferative compartment, requiring that the fold increase of transit rate in the differentiated compartment is higher than the fold increase of division rates in the proliferative compartment. This result agrees with an earlier prediction from Heenen et al. [60], showing that a relative growth in the proliferative compartment requires keratinocyte hyperproliferation and in the meantime an increased transit time in the differentiated compartment. A proportional increase in both TA-cell proliferation rate and transit rate ($\rho_{sc} = \rho_{tr}$) does not cause relatively differential growth of the two compartments unless difference exists between

increases of proliferating rates of stem cells and TA cells, $\rho_{sc} \neq \rho_{ta}$. Fast migration of differentiated keratinocytes also offsets overgrowth in the proliferative compartment. An important insight from the model is that increasing keratinocyte population in psoriasis is not merely caused by elevated proliferation rates but also requires the increase in growth capacity in the progenitor repertoire. Observed morphological remodeling of the psoriatic epidermis suggests increased growth niches for stem cells [73].

Similarly to Eq. (17), the epidermal turnover time can be approximated as the ratio of the total cell density to the rate of desquamation:

$$\begin{aligned} \tilde{\tau}_{\text{tot}} &\approx \frac{p_{\text{tot}}}{\alpha(p_{cc} + \rho_{de}\tilde{p}_{cc})} \\ &= \left(\frac{p_{sc} + \tilde{p}_{sc}}{p_{sc}\xi + \rho_{sc}\tilde{p}_{sc}} \frac{1}{g_h} + \frac{p_{sc}\xi + \frac{\rho_{sc}}{\rho_{ta}}\tilde{p}_{sc}}{p_{sc}\xi + \rho_{sc}\tilde{p}_{sc}} \right) \frac{1}{k_{2a} + 2k_{2s}} \\ &\quad + \frac{p_{sc}\xi + \frac{\rho_{sc}}{\rho_{tr}}\tilde{p}_{sc}}{p_{sc}\xi + \rho_{sc}\tilde{p}_{sc}} \left(\frac{1}{k_3} + \frac{1}{k_4} \right) \\ &\quad + \frac{p_{sc}\xi}{p_{sc}\xi + \tilde{p}_{sc}\rho_{sc}} \frac{1}{k_5} + \frac{p_{sc}\xi + \frac{\rho_{sc}}{\rho_{de}}\tilde{p}_{sc}}{p_{sc}\xi + \rho_{sc}\tilde{p}_{sc}} \frac{1}{\alpha}, \end{aligned}$$

which can be analyzed for the two psoriasis modes (quiescent or disease). At the quiescent mode, $\xi \approx 1$ and $p_{sc} \gg \tilde{p}_{sc}$, the

turnover time is approximated by

$$\tilde{\tau}_{\text{tot}} \approx \left(\frac{k_{2s} - \gamma_2}{k_{1a} + 2k_{1s}} + 1 \right) \frac{1}{k_{2a} + 2k_{2s}} + \frac{1}{k_3} + \frac{1}{k_4} + \frac{1}{k_5} + \frac{1}{\alpha},$$

converging back to τ_{tot} . At the disease mode, $\xi < 1$ and $p_{sc} \ll \tilde{p}_{sc}$. The turnover time is close to:

$$\tilde{\tau}_{\text{tot}} \approx \left(\frac{1}{\rho_{sc}g_h} + \frac{1}{\rho_{ta}} \right) \frac{1}{k_{2a} + 2k_{2s}} + \frac{1}{\rho_{tr}} \left(\frac{1}{k_3} + \frac{1}{k_4} \right) + \frac{1}{\rho_{de}} \frac{1}{\alpha}.$$

Both cases do not account for the relatively much smaller cell loss by the cytotoxic effect from the immune system. Compared to the turnover time of the healthy tissue τ_{tot} (Eq. 17), $\tilde{\tau}_{\text{tot}}$ of the psoriatic tissue is clearly shortened at each stage from the proliferative compartment (the first term) to differentiated compartment (the second term) and to the corneum (the third term). The turnover time of the granular layer is ignorable because of the minimal normal cell population.

ACKNOWLEDGMENTS

This work was supported by LVMH Recherche through Sprim Inc. and institutional fund to JY. We thank Weiren Cui, Eric Perrier, Michaël Shleifer, Gallic Beauchef and Delphine de Queral for helpful discussions.

-
- [1] W Montagna, AM Kligman, and KS Carlisle. 1992. *Atlas of normal human skin*. Springer-Verlag.
 - [2] T Burns, S Breathnach, N Cox, and C Griffiths, editors. 2010. *Rook's textbook of dermatology*. Wiley-Blackwell, 8th edition.
 - [3] GD Weinstein, JL McCullough, and P Ross. 1984. Cell proliferation in normal epidermis. *J. Invest. Dermatol.*, 82:623–628.
 - [4] M Loeffler, CS Potten, and HE Wichmann. 1987. Epidermal cell proliferation. II. A comprehensive mathematical model of cell proliferation and migration in the basal layer predicts some unusual properties of epidermal stem cells. *Virchows Arch. B Cell Pathol. Incl. Mol. Pathol.*, 53:286–300.
 - [5] LM Milstone. 2004. Epidermal desquamation. *J. Dermatol. Sci.*, 36:131–140.
 - [6] NJ Savill. 2003. Mathematical models of hierarchically structured cell populations under equilibrium with application to the epidermis. *Cell Prolif.*, 36:1–26.
 - [7] A Gandolfi, M Iannelli, and G Marinoschi. 2011. An age-structured model of epidermis growth. *J. Math. Biol.*, 62:111–141.
 - [8] D Stekel, J Rashbass, and ED Williams. 1995. A computer graphic simulation of squamous epithelium. *J. Theor. Biol.*, 175:283–293.
 - [9] N Grabe and K Neuber. 2005. A multicellular systems biology model predicts epidermal morphology, kinetics and Ca^{2+} flow. *Bioinformatics*, 21:3541–3547.
 - [10] T Sütterlin, S Huber, H Dickhaus, and N Grabe. 2009. Modeling multi-cellular behavior in epidermal tissue homeostasis via finite state machines in multi-agent systems. *Bioinformatics*, 25:2057–2063.
 - [11] T Sun, P McMin, S Coakley, M Holcombe, R Smallwood, and S MacNeil. 2007. An integrated systems biology approach to understanding the rules of keratinocyte colony formation. *J. R. Soc. Interface*, 4:1077–1092.
 - [12] S Adra, T Sun, S MacNeil, M Holcombe, and R Smallwood. 2010. Development of a three dimensional multiscale computational model of the human epidermis. *PLoS One*, 5:e8511.
 - [13] R Parisi, DPM Symmons, CEM Griffiths, and DM Ashcroft. 2013. Global epidemiology of psoriasis: A systematic review of incidence and prevalence. *J. Invest. Dermatol.*, 133:377–385.
 - [14] P Di Meglio, F Villanova, and FO Nestle. 2014. Psoriasis. *Cold Spring Harb. Perspect. Med.*, 4:a015354.
 - [15] G Denecker, P Ovaere, P Vandenaabee, and W Declercq. 2008. Caspase-14 reveals its secrets. *J. Cell Biol.*, 180:451–458.
 - [16] L De Rosa and M De Luca. 2012. Cell biology: Dormant and restless skin stem cells. *Nature*, 489:215–217.
 - [17] E Clayton, DP Doupé, AM Klein, DJ Winton, BD Simons, and PH Jones. 2007. A single type of progenitor cell maintains normal epidermis. *Nature*, 446:185–189.
 - [18] DP Doupé, AM Klein, BD Simons, and PH Jones. 2010. The ordered architecture of murine ear epidermis is maintained by progenitor cells with random fate. *Develop. Cell*, 18:317–323.
 - [19] G Mascré, S Dekoninck, B Drogat, KK Youssef, S Brohé, PA Sotiropoulou, BD Simons, and C Blanpain. 2012. Distinct contribution of stem and progenitor cells to epidermal maintenance. *Nature*, 489:257–262.

- [20] FM Watt and BLM Hogan. 2000. Out of eden: stem cells and their niches. *Science*, 287:1427–1430.
- [21] BD Simons and H Clevers. 2011. Strategies for homeostatic stem cell self-renewal in adult tissues. *Cell*, 145:851–862.
- [22] BD Simons and H Clevers. 2011. Stem cell self-renewal in intestinal crypt. *Exp. Cell Res.*, pages 2719–2724.
- [23] T Tumber, G Guasch, V Greco, C Blanpain, WE Lowry, M Rendl, and E Fuchs. 2004. Defining the epithelial stem cell niche in skin. *Science*, 303:359–363.
- [24] PB Warren. 2009. Cells, cancer, and rare events: Homeostatic metastability in stochastic nonlinear dynamical models of skin cell proliferation. *Phys. Rev. E*, 80:030903.
- [25] AM Klein, DP Doupé, PH Jones, and BD Simons. 2007. Kinetics of cell division in epidermal maintenance. *Phys. Rev. E*, 76:021910.
- [26] A Roshan and PH Jones. 2012. Act your age: Tuning cell behavior to tissue requirements in interfollicular epidermis. *Seminars Cell Develop. Biol.*, 23:884 – 889.
- [27] MP Alcolea and PH Jones. 2013. Tracking cells in their native habitat: lineage tracing in epithelial neoplasia. *Nature Rev. Cancer*, 13:161–171.
- [28] R Okuyama, K LeFort, and GP Dotto. 2004. A dynamic model of keratinocyte stem cell renewal and differentiation: role of the p21^{WAF1/Cip1} and Notch1 signaling pathways. *J. Investig. Dermatol. Symp. Proc.*, 9:248–252.
- [29] C Blanpain and E Fuchs. 2009. Epidermal homeostasis: a balancing act of stem cells in the skin. *Nat. Rev. Mol. Cell Biol.*, 10:207–217.
- [30] YC Hsu, L Li, and E Fuchs. 2014. Transit-amplifying cells orchestrate stem cell activity and tissue regeneration. *Cell*, 157:935–949.
- [31] M Heenen, S Thiriar, J-C Noël, and P Galand. 1998. Ki-67 immunostaining of normal human epidermis: comparison with 3H-thymidine labelling and PCNA immunostaining. *Dermatology*, 197:123–126.
- [32] M Heenen and P Galand. 1997. The growth fraction of normal human epidermis. *Dermatology*, 194:313–317.
- [33] R Morris and TS Argyris. 1983. Epidermal cell cycle and transit times during hyperplastic growth induced by abrasion or treatment with 12-O-tetradecanoylphorbol-13-acetate. *Cancer Res.*, 43:4935–4942.
- [34] FACM Castelijns, J Ezendam, MAHE Latijnhouwers, IMJJ Van Vlijmen-Willems, PLJM. Zeeuwen, MJP Gerritsen, PCM Van De Kerkhof, and PEJ Van Erp. 1998. Epidermal cell kinetics by combining *in situ* hybridization and immunohistochemistry. *Histochem. J.*, 30:869–877.
- [35] FA Castelijns, MJ Gerritsen, PE van Erp, and PC van de Kerkhof. 2000. Cell-kinetic evidence for increased recruitment of cycling epidermal cells in psoriasis: the ratio of histone and Ki-67 antigen expression is constant. *Dermatology*, 201:105–110.
- [36] M Laporte, P Galand, D Fokan, C de Graef, and M Heenen. 2000. Apoptosis in established and healing psoriasis. *Dermatology*, 200:314–316.
- [37] CE Gagna, NJ Chan, PN Farnsworth, HR Kuo, TR Kanthala, AH Patel, NH Patel, A Law, PP Patel, SA Richards, et al. 2009. Localization and quantification of intact, undamaged right-handed double-stranded B-DNA, and denatured single-stranded DNA in normal human epidermis and its effects on apoptosis and terminal differentiation (denucleation). *Arch. Dermatol. Res.*, 301:659–672.
- [38] EM Purcell. 1977. Life at low reynolds number. *Am. J. Phys.*, 45:3–11.
- [39] E Palsson. 2008. A 3-D model used to explore how cell adhesion and stiffness affect cell sorting and movement in multicellular systems. *J. Theo. Biol.*, 254:1–13.
- [40] X Li, AK Upadhyay, AJ Bullock, T Dicolandrea, J Xu, RL Binder, MK Robinson, DR Finlay, KJ Mills, CC Bascom, et al. 2013. Skin stem cell hypotheses and long term clone survival-explored using agent-based modelling. *Sci. Reports*, 3:1904.
- [41] G Schaller and M Meyer-Hermann. 2007. A modelling approach towards epidermal homeostasis control. *J. Theor. Biol.*, 247:554–573.
- [42] P Corcuff, C Bertrand, and JL Leveque. 1993. Morphometry of human epidermis *in vivo* by real-time confocal microscopy. *Arch. Dermatol. Res.*, 285:475–481.
- [43] G Plewig and RR Marples. 1970. Regional differences of cell sizes in the human stratum corneum. part i. *J. Invest. Dermatol.*, 54:13–18.
- [44] G Plewig. 1970. Regional differences of cell sizes in the human stratum corneum. ii. effects of sex and age. *J. Invest. Dermatol.*, 54:19–23.
- [45] N Kashibuchi, Y Hirai, K O’Goshi, and H Tagami. 2002. Three-dimensional analyses of individual corneocytes with atomic force microscope: morphological changes related to age, location and to the pathologic skin conditions. *Skin Res. Technol.*, 8:203–211.
- [46] R Marks, S Nicholls, and CS King. 1981. Studies on isolated corneocytes. *Int. J. Cosmet. Sci.*, 3:251–259.
- [47] A Giangreco, SJ Goldie, V Failla, G Saintigny, and FM Watt. 2009. Human skin aging is associated with reduced expression of the stem cell markers $\beta 1$ integrin and MCSP. *J. Invest. Dermatol.*, 130:604–608.
- [48] N Grabe and K Neuber. 2007. Simulating psoriasis by altering transit amplifying cells. *Bioinformatics*, 23:1309–1312.
- [49] GM Morris and JW Hopewell. 1990. Epidermal cell kinetics of the pig: a review. *Cell Prolif.*, 23:271–282.
- [50] J Bauer, FA Bahmer, J. Wörl, W Neuhuber, G Schuler, and M Fartasch. 2001. A strikingly constant ratio exists between Langerhans cells and other epidermal cells in human skin. A stereologic study using the optical disector method and the confocal laser scanning microscope. *J. Invest. Dermatol.*, 116:313–318.
- [51] SB Hoath and DG Leahy. 2003. The organization of human epidermis: functional epidermal units and phi proportionality. *J. Invest. Dermatol.*, 121:1440–1446.
- [52] PR Bergstresser, RJ Pariser, and JR Taylor. 1978. Counting and sizing of epidermal cells in normal human skin. *J. Invest. Dermatol.*, 70:280–284.
- [53] PR Bergstresser and JR Taylor. 1977. Epidermal ‘turnover time’ –a new examination. *Br. J. Dermatol.*, 96:503–506.
- [54] H Iizuka. 1994. Epidermal turnover time. *J. Dermatol. Sci.*, 8:215–217.
- [55] GD Weinstein and EJ van Scott. 1965. Autoradiographic analysis of turnover times of normal and psoriatic epidermis. *J. Invest. Dermatol.*, 45:257–262.
- [56] GL Grove and AM Kligman. 1983. Age-associated changes in human epidermal cell renewal. *J. Gerontol.*, 38:137–142.

- [57] GD Weinstein, JL McCullough, and PA Ross. 1985. Cell kinetic basis for pathophysiology of psoriasis. *J. Invest. Dermatol.*, 85:579–583.
- [58] SC Weatherhead, PM Farr, D Jamieson, JS Hallinan, JJ Lloyd, A Wipat, and NJ Reynolds. 2011. Keratinocyte apoptosis in epidermal remodeling and clearance of psoriasis induced by uv radiation. *J. Invest. Dermatol.*, 131:1916–1926.
- [59] GD Weinstein and JL McCullough. 1973. Cytokinetics in diseases of epidermal hyperplasia. *Annu. Rev. Med.*, 24:345–352.
- [60] M. Heenen, P. Galand, V Maertelaer, and Paul-Henri Heenen. 1987. Psoriasis: hyperproliferation cannot induce characteristic epidermal morphology. *Cell Prolif.*, 20:561–570.
- [61] T Simonart, M Heenen, and O Lejeune. 2010. Epidermal kinetic alterations required to generate the psoriatic phenotype: a reappraisal. *Cell Prolif.*, 43:321–325.
- [62] CJ Skerrow, DG Clelland, and D Skerrow. 1989. Changes to desmosomal antigens and lectin-binding sites during differentiation in normal human epidermis: a quantitative ultrastructural study. *J Cell Sci.*, 92:667–677.
- [63] RS Dawe, NJ Wainwright, H Cameron, and J Ferguson. 1998. Narrow-band (TL-01) ultraviolet B phototherapy for chronic plaque psoriasis: three times or five times weekly treatment? *Br. J. Dermatol.*, 138:833–839.
- [64] M Trehan and CR Taylor. 2002. Medium-dose 308-nm excimer laser for the treatment of psoriasis. *J. Amer. Acad. Dermatol.*, 47:701–708.
- [65] M Hartman, M Prins, OQJ Swinkels, JL Severens, Th. De Boo, GJ Van Der Wilt, PCM Van De Kerkhof, and PGM Van Der Valk. 2002. Cost-effectiveness analysis of a psoriasis care instruction programme with dithranol compared with uvb phototherapy and inpatient dithranol treatment. *Br. J. Dermatol.*, 147:538–544.
- [66] MA Lowes, AM Bowcock, and JG Krueger. 2007. Pathogenesis and therapy of psoriasis. *Nature*, 445:866–873.
- [67] CEM Griffiths and JNWN Barker. 2007. Pathogenesis and clinical features of psoriasis. *Lancet*, 370:263–271.
- [68] D Ludwig, DD Jones, and CS Holling. 1978. Qualitative analysis of insect outbreak systems: the spruce budworm and forest. *J Anim. Ecol.*, 47:315–332.
- [69] EJ Van Scott and TM Ekel. 1963. Kinetics of hyperplasia in psoriasis. *Arch. Dermatol.*, 88:373–381.
- [70] MA Lowes, M Suárez-Fariñas, and JG Krueger. 2014. Immunology of psoriasis. *Ann. Rev. Immunol.*, 32:227–255.
- [71] FK Doger, E Dikicioglu, F Ergin, E Unal, N Sendur, and M Uslu. 2007. Nature of cell kinetics in psoriatic epidermis. *J. Cutan. Pathol.*, 34:257–263.
- [72] A Menter and CEM Griffiths. 2007. Current and future management of psoriasis. *Lancet*, 370:272–284.
- [73] H Iizuka, H Takahashi, and A Ishida-Yamamoto. 2004. Psoriatic architecture constructed by epidermal remodeling. *J. Dermatol. Sci.*, 35:93–99.
- [74] JY Chang and PY Lai. 2012. Uncontrolled growth resulting from dedifferentiation in a skin cell proliferation model. *Phys. Rev. E*, 85:041926.
- [75] S Christley, B Lee, X Dai, and Q Nie. 2010. Integrative multicellular biological modeling: a case study of 3D epidermal development using GPU algorithms. *BMC Syst. Biol.*, 4:107.
- [76] A Gord, WR Holmes, X Dai, and Q Nie. 2014. Computational modelling of epidermal stratification highlights the importance of asymmetric cell division for predictable and robust layer formation. *J. Roy. Soc. Interface*, 11:20140631.
- [77] Y Liu, C Helms, W Liao, LC Zaba, S Duan, J Gardner, C Wise, A Miner, MJ Malloy, CR Pullinger, et al. 2008. A genome-wide association study of psoriasis and psoriatic arthritis identifies new disease loci. *PLoS Genet.*, 4:e1000041.
- [78] RP Nair, KC Duffin, C Helms, J Ding, PE Stuart, D Goldgar, JE Gudjonsson, Y Li, T Tejasvi, BJ Feng, et al. 2009. Genome-wide scan reveals association of psoriasis with IL-23 and NF- κ B pathways. *Nat. Genet.*, 41:199–204.
- [79] CT Jordan, L Cao, E Roberson, S Duan, CA Helms, RP Nair, KC Duffin, PE Stuart, D Goldgar, G Hayashi, et al. 2012. Rare and common variants in CARD14, encoding an epidermal regulator of NF- κ B in psoriasis. *Am. J. Hum. Genet.*, 90:796–808.
- [80] LC Tsoi, SL Spain, J Knight, E Ellinghaus, PE Stuart, F Capon, J Ding, Y Li, T Tejasvi, JE Gudjonsson, et al. 2012. Identification of 15 new psoriasis susceptibility loci highlights the role of innate immunity. *Nat. Genet.*, 44:1341–1348.
- [81] E Roberson and AM Bowcock. 2010. Psoriasis genetics: breaking the barrier. *Trends Genetics*, 26:415–423.
- [82] FO Nestle, DH Kaplan, and J Barker. 2009. Psoriasis. *New Eng. J. Med.*, 361:496–509.
- [83] DJ Fife, JM Waller, EW Jeffes, and JY Koo. 2007. Unraveling the paradoxes of HIV-associated psoriasis: a review of T-cell subsets and cytokine profiles. *Dermatol. Online J.*, 13:4.
- [84] N Morar, SA Willis-Owen, T Maurer, and CB Bunker. 2010. HIV-associated psoriasis: pathogenesis, clinical features, and management. *Lancet Infect. Dis.*, 10:470–478.
- [85] R Queiro, P Tejón, S Alonso, and P Coto. 2014. Age at disease onset: a key factor for understanding psoriatic disease. *Rheumatology*, 53:1178–1185.
- [86] JH Lee, HT An, JH Chung, KH Kim, HC Eun, and KH Cho. 2002. Acute effects of uvb radiation on the proliferation and differentiation of keratinocytes. *Photodermatol. Photoimmunol. Photomed.*, 18:253–261.
- [87] S Del Bino, C Vioux, P Rossio-Pasquier, A Jomard, M Demarchez, D Asselineau, and F Bernerd. 2004. Ultraviolet b induces hyperproliferation and modification of epidermal differentiation in normal human skin grafted on to nude mice. *Br. J. Dermatol.*, 150:658–667.
- [88] E Rácz, EP Prens, D Kurek, M Kant, D de Ridder, S Mourits, EM Baerveldt, Z Ozgur, W FJ van IJcken, JD Laman, FJ Staal, and L van der Fits. 2011. Effective treatment of psoriasis with narrow-band uvb phototherapy is linked to suppression of the ifn and th17 pathways. *J. Invest. Dermatol.*, 131:1547–1558.
- [89] BST Wong, BAL Hsu, and MDW Liao. 2013. Phototherapy in psoriasis: a review of mechanisms of action. *J. Cutan. Med. Surg.*, 17:6–12.
- [90] G Driessens, B Beck, A Caauwe, BD Simons, and C Blanpain. 2012. Defining the mode of tumour growth by clonal analysis. *Nature*, 488:527–530.

SUPPLEMENTARY MATERIALS

Computation of population kinetics model

The central transition pathway of the epidermis renewal can be computed in two alternative ways (Fig. S1) to obtain the *deterministic* or *stochastic dynamics* of the system. The mathematical equations [the ordinary differential equations (ODEs) or the master equations] of the system for the normal tissue can be found in Table 1 of the paper.

Deterministic simulation — The deterministic model describes cell populations by a set of ODEs with the cell densities as the state variables according to the rate processes in the central transition pathway. Numerically integrating the ODEs obtains trajectories of the cell density distribution over all individual cell types.

Stochastic simulation — In this case, rate processes in the central transition pathway are sampled by the Gillespie's algorithm [1] to generate probabilistic cellular events sequentially in time. An individual cell process is chosen by a probability proportional to the rate of the process, and the occurrence time interval is sampled as in a Poissonian process with a mean rate equal to the accumulated rate of all processes in the system. Time series of cell events generated by the stochastic simulation are fed to the agent-based cell migration model to simulate and visualize the spatiotemporal organization of keratinocytes in the epidermis.

Computation of agent-based cell migration model

Simulation of the cell migration model is coupled with the stochastic simulation of the cell population kinetics model described in the previous section. Because the cell population kinetics is treated independently from the cell migration in our model, the stochastic simulation of population dynamics can be completed before simulating the cell migration, and the generated cellular events of proliferation, differentiation, apoptosis and desquamation can be stored and later embedded into the time series of migration events.

Repulsive force — The amount of repulsive force \mathbf{F}_{ij}^r is assumed to be proportional to the overlapping area S_{ij} and the direction of the force is along the line connecting the cell centers of cells i and j . At time t , the two orthogonal components $\mathbf{F}_{ij}^r(t) \equiv [F_{ij}^{r,x}(t), F_{ij}^{r,y}(t)]$ is given as

$$F_{ij}^{r,x}(t) = kS_{ij}(t) \cos \theta_{ij}, \text{ and } F_{ij}^{r,y}(t) = kS_{ij}(t) \sin \theta_{ij}, \quad (\text{S1})$$

where θ_{ij} is the angle of vector \mathbf{F}_{ij}^r and k is a constant assumed identical for all cell types.

In theory, the overlapping area between two ellipsoids can be precisely calculated by a numerical integration. To increase computational efficiency, S_{ij} (note that $S_{ij} = S_{ji}$) is however approximated by the overlap between the two cells as if they are rectangles with widths and heights identical to the corresponding ellipsoids. An overlap happens between cells i and j if the following two conditions hold:

$$|x_i - x_j| < \frac{w_i + w_j}{2}, \quad \text{and } |y_i - y_j| < \frac{h_i + h_j}{2}, \quad (\text{S2})$$

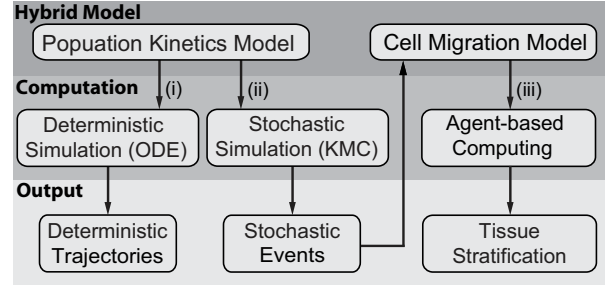


FIG. S1. **Schemes of model computation.** Kinetics of the central transition pathway of the epidermis renewal can be computed by one of the two numerical methods: (i) integrating the system of ODEs, or (ii) stochastic simulation algorithm (SSA). As a third option (iii), the spatio-temporal dynamics of the epidermis renewal can be computed and visualized by incorporating cell events generated by the stochastic simulation into the cell migration model.

where h_i and w_i are height and width of cell i , respectively. The width and height, w_{ij} and h_{ij} , of the overlap rectangle can then be calculated as

$$w_{ij} = \min\left\{\frac{w_i + w_j}{2} - |x_i - x_j|, w_i, w_j\right\} \quad (\text{S3})$$

$$h_{ij} = \min\left\{\frac{h_i + h_j}{2} - |y_i - y_j|, h_i, h_j\right\}, \quad (\text{S4})$$

and the overlap area is approximated as $S_{ij} \approx w_{ij}h_{ij}$.

Adhesive force — We adapt the treatment of cell-cell adhesive force from Palsson model [2] and Li et al. [3]. The adhesive force between two adjacent cells i and j , \mathbf{F}_{ij}^a , is a biphasic function of the cell-cell distance and the direction of the force is along with the line connecting the cell centers. We have the following equation for \mathbf{F}_{ij}^a (see Fig. S2 for plots of force-distance relationship):

$$F_{ij}^a = -\sigma \left[\left(\frac{g_{ij}}{r} + c_1 \right) e^{-\zeta \left(\frac{g_{ij}}{r} + c_1 \right)^2} - c_2 e^{-\zeta \left(\frac{g_{ij}}{r} \right)^2} \right], \quad (\text{S5})$$

where $c_1 = 1/\sqrt{2\zeta}$, $c_2 = c_1 e^{-1/2}$, r is the average radius of cells, g_{ij} is the distance between cell i and cell j . The adhesion factor σ is a measure of the strength of the adhesion.

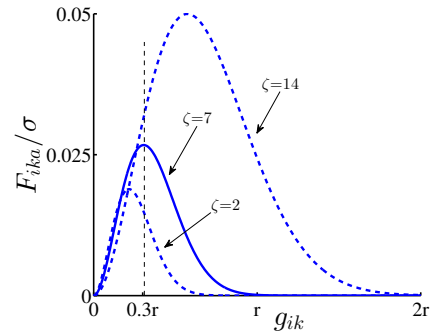


FIG. S2. **Adhesive force.** The normalized adhesive force (F_{ik}^a/σ) related the cell-cell distance under different ζ values. The adhesive force decreases to zero at $\zeta = 7$ when the cell-cell distance exceeds the cell radius r .

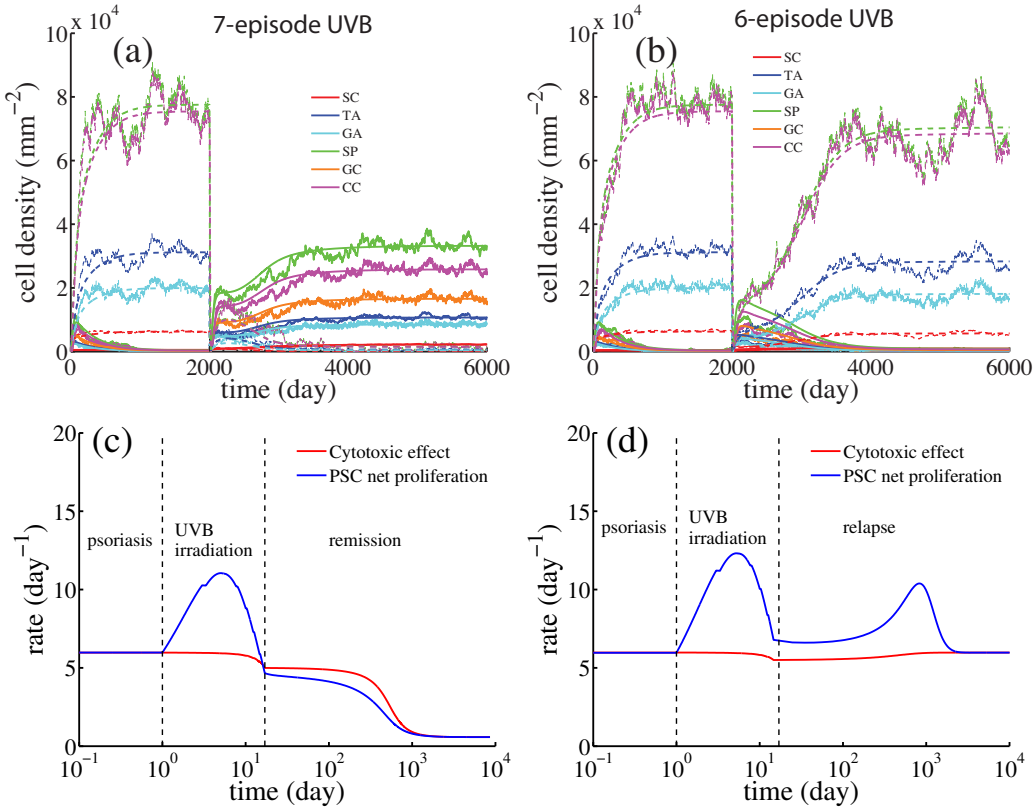


FIG. S3. **Psoriasis phototherapy by multi-episode UVB irradiation.** (a) 7-episode and (b) 6-episode UVB irradiation treatments. The model simulated an area of length 5 mm \times width 0.01 mm = 0.05 mm² (i.e., a single-cell sheet of the epidermis). Simulations started with a mixed population of normal (solid) and psoriatic (dashed) stem cells (about a 20:200 ratio). Temporal evolution of the cytotoxic killing rate and psoriatic stem cell (PSC) net proliferation rate (selfproliferation rate - symmetric division rate) in (c) 7-episode and (d) 6-episode UVB irradiation. Note that compared to (a) and (b), time axes are shifted in plots (c) and (d) to remove the initial transient dynamics to psoriatic homeostasis. The UVB treatments follow the same protocol described in the main text (Fig. 6). Parameter values used in the simulations are listed in the main text (Table 3).

The density of desmosomes (typical cell junctions) has a nonuniform distribution across different layers indicating varying adhesion strength in different cell types [3–5]. σ can be adjusted for different keratinocytes to reflect this variation. We assume that the adhesion strength in proliferating cells is the strongest and decreases from inner to outer layer in non-proliferating compartment due to decreased density of desmosomes. For example, the corneocytes has reduced adhesion as Skerrow et al. [4] reported that the ratio of desmosome densities of differentiated layers and corneocyte layer was about 6. For calculating the adhesion forces between different cell types a and b , the mean $\sigma_{ab} = (\sigma_a + \sigma_b)/2$ is used. We also note that stem cells are located on niches and move laterally along the basement membrane.

Parameter ζ is usually assumed to be 7 with which the adhesive force is almost zero when the distance between two cells is larger than the mean cell radius r . The force increases as the distance increases from zero and reaches a max force when the distance is about $0.3r$ (see Fig. S2). As the distance increases further, the adhesion declines to zero. For computational efficiency, the distance between two adjacent cells is approximated by the shortest distance between cells represented as rectangles with widths and heights identical

to the corresponding ellipsoids. The cell-cell distance is calculated by

$$g_{ij} = \sqrt{x_{ij}^2 + y_{ij}^2}. \quad (\text{S6})$$

where

$$x_{ij} = \max\{|x_i - x_j| - \frac{w_i}{2} - \frac{w_j}{2}, 0\} \quad (\text{S7})$$

$$y_{ij} = \max\{|y_i - y_j| - \frac{h_i}{2} - \frac{h_j}{2}, 0\} \quad (\text{S8})$$

The equation of motion for cell migration

$$\mu \frac{d\mathbf{x}_i}{dt} + \mathbf{F}_i^r + \mathbf{F}_i^a = 0, \quad (\text{S9})$$

$$\mathbf{F}_i^r = \sum_{j \in \mathcal{O}(i)} \mathbf{F}_{ij}^r, \quad \mathbf{F}_i^a = \sum_{j \in \Omega(i)} \mathbf{F}_{ij}^a \quad (\text{S10})$$

can be numerically solved for individual cells by a finite difference method. With a small time step Δt_c , given the location of cell i at time t , $\mathbf{x}_i(t)$, one can estimate the cell location $\mathbf{x}_i(t + \Delta t_c)$ as a first-order approximation,

$$\mathbf{x}_i(t + \Delta t_c) \approx \mathbf{x}_i(t) - \frac{\mathbf{F}_i^r(t) + \mathbf{F}_i^a(t)}{\mu} \Delta t_c. \quad (\text{S11})$$

TABLE V. Operation rules for cell events in the cell migration model

Event	Operation rule
SC \rightarrow SC + TA	Randomly divide a SC and place daughter cells beside each other [†]
SC \rightarrow SC + SC	Randomly divide a SC and place daughter cells beside each other [†]
SC \rightarrow TA + TA	Randomly divide a SC and place daughter cells beside each other [†]
TA \rightarrow SC	Randomly replace a (normal) TA cell or replace the lowest (psoriatic) TA cell by a SC [†]
TA \rightarrow TA + TA	Randomly divide a TA cell and place daughter cells beside each other
TA \rightarrow GA + TA	Randomly divide a TA cell at the boundary and place daughter cells beside each other
TA \rightarrow GA + GA	Divide the outmost TA cell and place daughter cells beside each other
GA \rightarrow TA	Randomly replace a GA cell at the boundary by a TA
Differentiation	Replace the outmost cell by a cell of the new type
Apoptosis	Randomly choose a cell of proper type and remove
Desquamation	Remove the outmost CC

[†]SCs and normal TA cells only undergo lateral motion along the basement membrane.

The basement membrane — Cell migration is bounded by the basement membrane, whose morphology and remodeling must be accounted for. The undulant basement membrane at location x , is generated by a shifted Gaussian function:

$$-H(x) = Ae^{-(x-x_0)^2/\sigma_s^2} - B, \quad (\text{S12})$$

where parameters A , B and σ_s model the depth and width of the rete ridge. The variable x_0 controls the location of a rete ridge along the basement membrane. Simulations introduce 10% fluctuations in parameters A and σ_s and in cell sizes (width and height) about the means when a new (or newly differentiated) cell is produced. Periodical boundary condition was used to process cell motion across the left and right boundaries. In the normal tissue, proliferating cells including stem cells and TA cells only undergo lateral movement along the basement membrane.

The complete algorithm that simulates the stochastic spatiotemporal dynamics of the epidermis renewal is outlined as follows.

1. Simulate the cell population kinetics model with the Gillespie's algorithm, and store the time series of cell events.
2. Specify the basement membrane and coordinates of the initial cell population and calculate mechanical forces exerted on each individual cells using Eqs. (S1), (S5) and (S10), and set the simulation time $t = 0$ and the time step Δt_c .
3. Execute available cell events within $[t, t + \Delta t_c]$ according to the rules described in Table V.
4. Calculate mechanical forces for all affected cells and migrate cells to the new coordinates calculated by Eq. (S11), and advance the time $t \leftarrow t + \Delta t_c$.
5. Iterate Step 3 until stop.

The model simulation and visualization algorithms are implemented in the Matlab and Java Language and are available at <http://www.picb.ac.cn/stab/epidermal.html>.

Simulations of psoriatic epidermal homeostasis and treatment by UVB irradiation

Both deterministic and stochastic dynamics of a psoriasis plaque and its post-treatment remission after 7-episode UVB irradiations and relapse after 6-episode UVB irradiation are shown in Fig. S3(a) and (b). The dynamic interplays between the cytotoxic effect by the immune system and the psoriatic stem cell proliferation are shown in Fig. S3(c) and (d) for the 7-episode (effective) and 6-episode (ineffective) treatments, respectively. At the pretreatment homeostasis, the cytotoxic effect on PSC (the killing rate) balances the net PSC proliferation rate. Upon the start of a UVB irradiation, the PSC net proliferation initially increases due to increased self-proliferation that tends to fill the SC niche capacity, but however drops back during later UVB episodes because the healthy SCs proliferation picks up the competition for the niches. In this phase, the cytotoxic rate gradually drifts lower because of the reduced PSC population. A successful treatment (7-episode in Fig S3(c)) brings the net PSC proliferation below the cytotoxicity at the end of the therapy and from there the plaque eventually achieves a remission where two rates balance again at the quiescent mode homeostasis. By contrast, in a less-dosed regimen (6-episode in Fig S3(d)), the net PSC proliferation stays higher than the cytotoxicity throughout. Once the treatment stops, PSC proliferation progressively outcompetes and healthy SC proliferation for the niches and the plaque relapses in the end.

Fig. S4 shows a few snapshots of 2D tissue stratification during a simulation. Simulation movies are available at URL: <http://www.picb.ac.cn/stab/epidermal.html>.

In the psoriatic tissue, because of high density of proliferating cells, TA cells are allowed to migrate within a larger (but restricted) area, within a band parallel to the basement membrane. The height of the band is modulated by the density of proliferating cells with a $15 \mu\text{m}$ increment (decrement) for every 18000 mm^{-2} increase (decrease) in proliferating cell density.

In comparison to a fixed rete ridge, the dynamics of rete ridge remodeling is considered in the psoriasis model. We assume that the rete ridge remodels between normal and psoriatic structures according to proportions of normal and psoriatic cells. The fraction of normal progenitor cells is

defined as

$$r = \frac{\text{normal SC + TA cells}}{\text{total SC + TA cells}}, \quad (\text{S13})$$

Let y be the rete ridge height in time and Y is the target homeostatic rete ridge height. We assume that the dynamics of the rete ridge follows a first-order dynamics

$$\tau \frac{dy}{dt} = Y - y, \quad (\text{S14})$$

where τ is the time constant for the dynamics. We further assume Y is linearly regulated by r :

$$Y = Y_{\max} - (Y_{\max} - Y_{\min})r, \quad (\text{S15})$$

where Y_{\max} (Y_{\min}) is reached at $r = 0$ ($r = 1$).

Eq. (S14) is numerically solved by the finite difference method as follows:

$$y(t + \Delta t_{\text{bm}}) = \frac{Y(t) - y(t)}{\tau} \Delta t_{\text{bm}} + y(t), \quad (\text{S16})$$

where $Y(t)$ is calculated from Eq. (S15).

We set $Y_{\min} = 40 \mu\text{m}$ to match the healthy tissue when normal stem cells dominate at the homeostasis and $Y_{\max} = 126 \mu\text{m}$, about 3 times higher than the normal epidermis. Based on data from successful UVB treatments showing that psoriasis plaques achieved remission in about 3-4 months [6–8], we set the time constant $\tau = 100$ day and Δt_{bm} was chosen as 20 day. In a simulation, whenever the basement membrane remodels, all stem cells and normal TA cells are relocated along with the membrane accordingly and other cells stay above the basement membrane.

Identification of model parameters

We archive parameter values in Table 2 and 3 in the main text. The literature that reported parameter values

or provided information to derive the parameter values is listed in the tables. For example, cell sizes of keratinocytes at different stages are reported in histology studies, and rate constants for proliferation and differentiation are assigned based on measurements (such as the stem cell proliferation rate) or identified from cell density distribution data and the measured epidermal turnover time. We list multiple references for a parameter value if available for confirmation, but we acknowledge that the reference list may not be exhaustive. We also note that these parameter values serve as references and should not be considered as fixed because of variations of the epidermis homeostasis at skin location, age, gender and pathological conditions and uncertainties in experimental measurements.

Parameters that are not measured are estimated or assumed (as indicated in the Tables). Assumed parameter values are justifiable based on available information. For example, the stem cell growth capacity $p_{\text{sc}}^{\text{max}}$ in the healthy tissue is assumed as $4.5\text{e}3 \text{ mm}^2$, about 2 times the homeostatic density, considering significant loss of stem cells through symmetric division and apoptosis. In comparison, the growth capacity in the psoriatic tissue is extended ($\lambda = 3.5$ fold larger), which was suggested by the histology data that showed extending rete ridge. Correspondingly, the maximum rete ridge height Y_{\max} is assumed more than 3 times that of the healthy one. Parameters such as the maximum cytotoxic rate K_p have not been experimentally measured, which is chosen to predict a psoriasis mode (e.g., $K_p = 6 \text{ mm}^{-2}\text{day}^{-1}$ is chosen to parameterize a switchable psoriatic tissue).

-
- [1] DT Gillespie. 2007. Stochastic simulation of chemical kinetics. *Annu. Rev. Phys. Chem.*, 58:35–55.
 - [2] E Palsson. 2008. A 3-D model used to explore how cell adhesion and stiffness affect cell sorting and movement in multicellular systems. *J. Theo. Biol.*, 254:1–13.
 - [3] X Li, AK Upadhyay, AJ Bullock, T Dicolandrea, J Xu, RL Binder, MK Robinson, DR Finlay, KJ Mills, CC Bascom, et al. 2013. Skin stem cell hypotheses and long term clone survival-explored using agent-based modelling. *Sci. Reports*, 3.
 - [4] CJ Skerrow, DG Clelland, and D Skerrow. 1989. Changes to desmosomal antigens and lectin-binding sites during differentiation in normal human epidermis: a quantitative ultrastructural study. *J Cell Sci.*, 92:667–677.
 - [5] RA Foty and MS Steinberg. 2005. The differential adhesion hypothesis: a direct evaluation. *Develop. Biol.*, 278:255–263.
 - [6] RS Dawe, NJ Wainwright, H Cameron, and J Ferguson. 1998. Narrow-band (TL-01) ultraviolet B phototherapy for chronic plaque psoriasis: three times or five times weekly treatment? *Br. J. Dermatol.*, 138:833–839.
 - [7] M Trehan and CR Taylor. 2002. Medium-dose 308-nm excimer laser for the treatment of psoriasis. *J. Amer. Acad. Dermatol.*, 47:701–708.
 - [8] M Hartman, M Prins, OQJ Swinkels, JL Severens, Th. De Boo, GJ Van Der Wilt, PCM Van De Kerkhof, and PGM Van Der Valk. 2002. Cost-effectiveness analysis of a psoriasis care instruction programme with dithranol compared with uvb phototherapy and inpatient dithranol treatment. *Br. J. Dermatol.*, 147:538–544.
 - [9] H Iizuka, H Takahashi, and A Ishida-Yamamoto. 2004. Psoriatic architecture constructed by epidermal remodeling. *J. Dermatol. Sci.*, 35:93 – 99.
 - [10] SC Weatherhead, PM Farr, D Jamieson, JS Hallinan, JJ Lloyd, A Wipat, and NJ Reynolds. 2011. Keratinocyte apoptosis in epidermal remodeling and clearance of psoriasis induced by uv radiation. *J. Invest. Dermatol.*, 131:1916–1926.

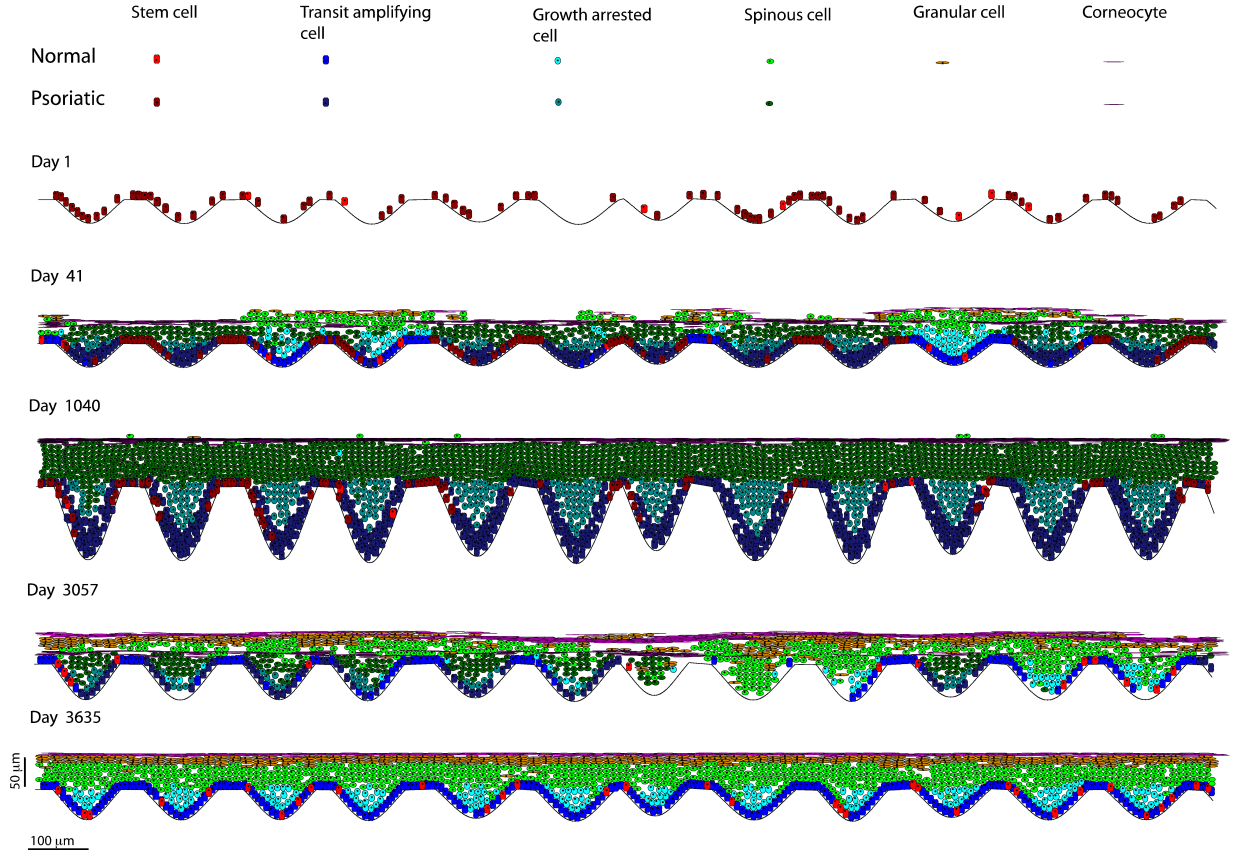


FIG. S4. **Snapshots of simulated psoriatic epidermis under a 7-episode UVB irradiation (visualization of simulation in Fig. S3(a)).** Each snapshot shows two fifth of the simulated length of 5 mm. Same types of normal and psoriatic cells are identically colored but with different contrasts as annotated in the top panel. The simulation starts at day 1 with a mixed initial population of normal (20) and psoriatic (200) stem cells randomly distributed on the basement membrane. The simulated tissue grows through a transient phase (Day 41, a mix of normal and psoriatic cells are visible. Note that in this phase the disparity in growth rates of normal and psoriatic keratinocytes generate morphological heterogeneity in the epidermis.) to achieve a parallel homeostasis between normal and psoriatic keratinocytes (Day 1040, most cells are psoriatic and the epidermis thickens with extended rete ridges). Episodes of UVB irradiation reduce the cell population (Day 3057, at the early recovery with normal cells). After recovery, the epidermis is composed primarily of normal keratinocytes (Day 3635). In simulation, the rete ridge in psoriasis is dynamically extended (see the text for the dynamic model of rete ridge) to reach a height of $126 \mu\text{m}$ at the homeostasis (about 3-4 times larger than that of the normal tissue [9, 10]). The simulation sets a small $\Delta t_c = 0.002$ day to ensure accurate numerical integration and to bracket within each migration time step only a few (about 2) cellular events happen along a unit epidermal length (1 mm). Psoriatic TA cells are not anchored but migrate within a confined region above the basement membrane with a height depending on the TA cell density.